ORIGINAL RESEARCH

# Potential of oil palm frond cellulose nanocrystals-activated carbon hydrogel beads for the removal of paracetamol from aqueous media

Nor Najhan Idris · Tuan Sherwyn Hamidon · Nor Salmi Abdullah · Lisman Suryanegara · M. Hazwan Hussin

**Abstract** Water pollution via pharmaceutical drugs such as paracetamol has been a highly concerning issue, and effective measures must be taken to treat these aquatic contaminants. Hence, the present study explored the use of cellulose nanocrystals (CNC) isolated from oil palm fronds (OPF), combined with commercial activated carbon (AC) to produce OPF CNC-AC hydrogel beads for paracetamol removal from aqueous media. The BET analysis showed that the OPF CNC-AC hydrogel beads possess a high BET surface area of 85.19 $m^2$ $g^{-1}$. FTIR analysis showed several peaks had higher intensities and were slightly shifted than those before adsorption, and the SEM analysis confirmed these findings. Adsorption studies were conducted to infer how solution pH, contact time,

and initial paracetamol concentration affect the adsorption behaviour. It was revealed that the adsorption studies of paracetamol could be achieved at 0.6 g of adsorbent dosage, at a pH 3 with a contact time of 170 min under room temperature. Meanwhile, the pseudo-second order kinetic model and Langmuir isotherm model revealed the best correlation for the adsorption of paracetamol with a $q_{max}$ value of 21.34 mg $g^{-1}$ and Gibbs free energy of adsorption ($\Delta G$) of $-10.27$ kJ $mol^{-1}$. Thus, monolayer adsorption was thought to occur at the surface of OPF CNC-AC hydrogel beads. This study suggests that OPF CNC-AC hydrogel beads could be a viable adsorbent for paracetamol removal from water used for consumption, which showed an efficiency of up to 79.98% in eliminating paracetamol dissolved in enriched aqueous solutions.

N. N. Idris · T. S. Hamidon · M. H. Hussin (✉)
Materials Technology Research Group (MaTReC), School of Chemical Sciences, Universiti Sains Malaysia, 11800 Minden, Penang, Malaysia
e-mail: mhh.usm@gmail.com; mhh@usm.my

N. S. Abdullah
National Hydraulic Research Institute of Malaysia (NAHRIM), Jalan Putra Permai, Seri Kembangan, Selangor Darul Ehsan, Minden, Penang, Malaysia

L. Suryanegara
Indonesian Institute of Sciences (LIPI), Jl. Raya Bogor Km 46, Cibinong, Bogor 16911, Jawa Barat, Indonesia

## Graphical Abstract
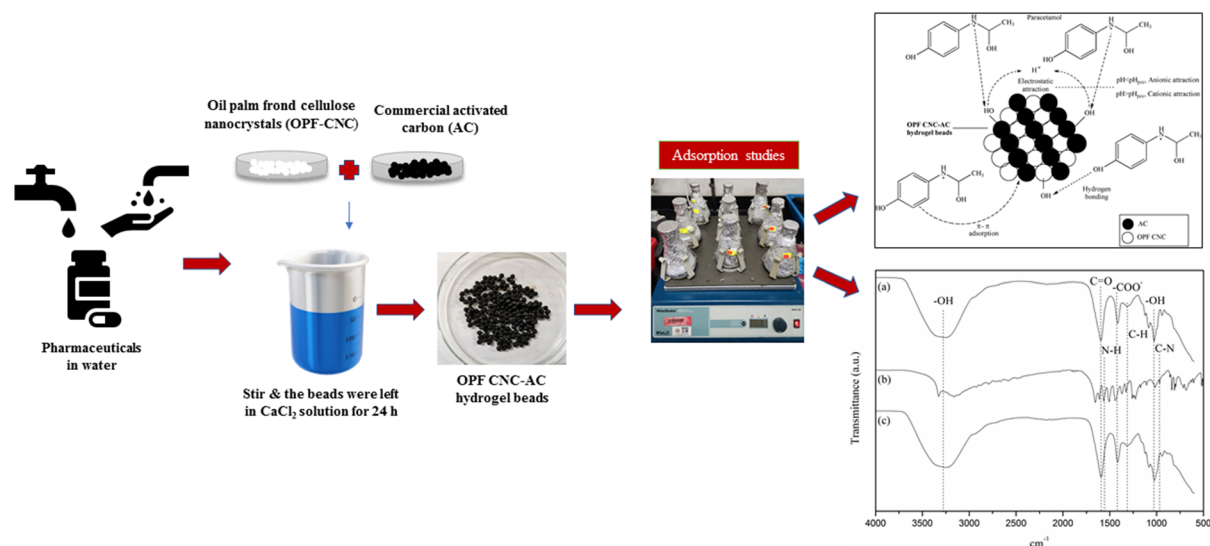
## Introduction

First and foremost, water is ultimately the essential compound on earth. This is due to the fact that it is required by all plants and animals. As a result of the growing population size and increased industrial enterprise, the demand for clean water has increased (Mohammed et al. 2015). However, the development and the use of pharmaceutical compounds to treat human and veterinary diseases have rapidly increased, causing the water to be contaminated with organic compounds (Chen et al. 2013). A part of these compounds is excreted through faeces or urine from the body. In recent years, direct discharge such as pharmaceutical industry wastewater and indirect discharge like municipal and hospital effluents have become increasingly recognized emerging issues due to the harmful effects of pharmaceutical compounds on human and environmental health (Patel et al. 2019). Lei et al. (2015) pointed out that emerging pollutants are substances not protected by current water regulations but are considered a risk to ecosystems and human health.

Pharmaceuticals are natural or synthetic chemicals that can be used in prescription drugs, over-the-counter medicinal drugs, and veterinary medicines that contain active ingredients intended to have pharmacological effects and confer significant social benefits (Mukoko 2016). After use, certain medications are released into the environment, while others are discarded as unused or expired items during manufacturing (Rogowska et al. 2019). Pharmaceutical compounds can navigate their way to wastewater collection systems that are ultimately discharged into wastewater facilities (Aydin and Talinli 2013; Yan et al. 2014). As a result, residual amounts in treated water have accumulated in drinking water (Rivera-Utrilla et al. 2013). Even at relatively low doses, the presence of pharmaceuticals in the aquatic environment still can affect non-target individuals and organisms (Coimbra et al. 2018). Several studies have stated that pharmaceutical compounds and their components are widely found ranging from ng/L to µg/L of concentrations in wastewater, sewage, surface water,
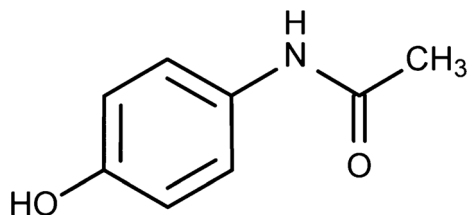


**Fig. 1** Molecular structure of paracetamol

groundwater, and even drinking water (Mompelat et al. 2009; Sim et al. 2010).

Paracetamol (Fig. 1) is one of the pharmaceutical compounds found in natural waters due to its widespread consumption. Acetaminophen, often known as paracetamol, is a non-steroidal anti-inflammatory medicine used worldwide for pain treatment and fever reduction (De Laurentiis et al. 2014). This antipyretic medicine is easily and readily available even without a medical prescription. Around 58–68% paracetamol is eliminated from the body when consumed in therapeutic dosage. Thus, paracetamol concentration may be significant in wastewater and water supplies (de Luna et al. 2013). This active pharmaceutical compound used by both humans and animals is not fully metabolized within their bodies. As a result, they are excreted by urine or faeces and join wastewater as biologically active substances along with metabolization products (Snelgrove 2017). Thus, people are exposed to these active pharmaceutical compounds via their potable water or through bioaccumulation in the food web. Paracetamol is reasonably stable at a regular dose, but at overdoses, the concentration has some hazards and may cause liver failure, gastrointestinal disease, centrilobular liver necrosis, and ultimately hepatotoxic potential (Bhushan and Apte 2019). It is a common pharmaceutical that has been found in wastewater at various concentrations all around the world (Gracia-Lor et al. 2012). In wastewater treatment plant influent samples, paracetamol was found in the range of 1.746 43.223 μg/L. Meanwhile, in wastewater treatment plant effluent samples, it was found in the range of 0.025–4.319 μg/L (Wadhah Hassan 2017).

Effluents containing pharmaceutical compounds should be handled properly to prevent harmful effects on humans and the environment. Conventional wastewater treatment plants are typically designed to eliminate suspended solids, the need for biochemical oxygen demand (BOD), and pathogenesis. Therefore, they cannot eliminate pharmaceutical compounds effectively (Mashayekh-Salehi and Moussavi 2016). Several chemical, biological, and physical methods can be used to extract pharmaceutical compounds from polluted water, such as biodegradation, membrane filtration, coagulation, and adsorption. Mashayekh-Salehi and Moussavi (2016) stated that adsorption is among the most promising strategies for eliminating pharmaceutical compounds due to its high

potential for adsorption, low energy cost, and environmental friendliness. The evolution of new low-cost adsorbents derived from renewable resources has been motivated due to the high cost and energy associated with the manufacture and regeneration of the adsorbent (Mohammed et al. 2015). Some examples of green adsorbents that have been reported are rice hulls (Mukoko 2016), kenaf (Macías-García et al. 2019), tilia leaves (Husein et al. 2019), greenwood chips (Liyanage et al. 2020) and corncobs (Fu et al. 2020).

Oil palm is one of Malaysia's most substantial commercial crops. The oil palm (*Elaeis guineensis*) is widely grown as a source of oil throughout West and Central Africa and Malaysia, Indonesia, and Thailand (Barthel et al. 2018). The palm oil industry is among the essential agro-industries in Malaysia, and it produces enormous amounts of solid oil palm waste, including oil palm fronds (OPF). Such solid wastes have no economic value and cause a significant issue in terms of disposal. Through the optimum utilization of oil palm biomass, all these problems can be reduced, and these lignocellulosic materials can be used for great value-added products by biological, chemical, and physical developments (Diyanilla et al. 2020). Hussin et al. (2016) have reported using lignocellulosic biomass such as OPF as a green adsorbent. Lignocellulosic oil palm biomass (OPB) is abundant with carbohydrates, and they consist of organic compounds, such as cellulose, hemicelluloses, and lignin (Diyanilla et al. 2020; Maya et al. 2016). Therefore, using oil palm solid waste as a low-cost adsorbent might benefit from an economic and environmental perspective (Setiabudi et al. 2016). A high-value by-product can be obtained from OPB, which can be used as energy sources, fertilizers, animal food, furniture, and paper sectors (bin Abas et al. 2004; Dungani et al. 2018). This situation approaches the manufacturing of green materials that draw the attention and curiosity of researchers to protect the environment (Haafiz et al. 2013). According to Tan et al. (2018), OPF has been used as a green adsorbent for methylene blue dye removal. Recently, there was a study of chitosan/biochar hydrogel beads on the adsorption of pharmaceutical contaminants such as paracetamol and ciprofloxacin (Afzal et al. 2018; Vakili et al. 2019a). However, no comprehensive research reported on the utilization of hydrogel beads extracted from oil palm biomass such as OPF for the adsorption of paracetamol in aqueous media.
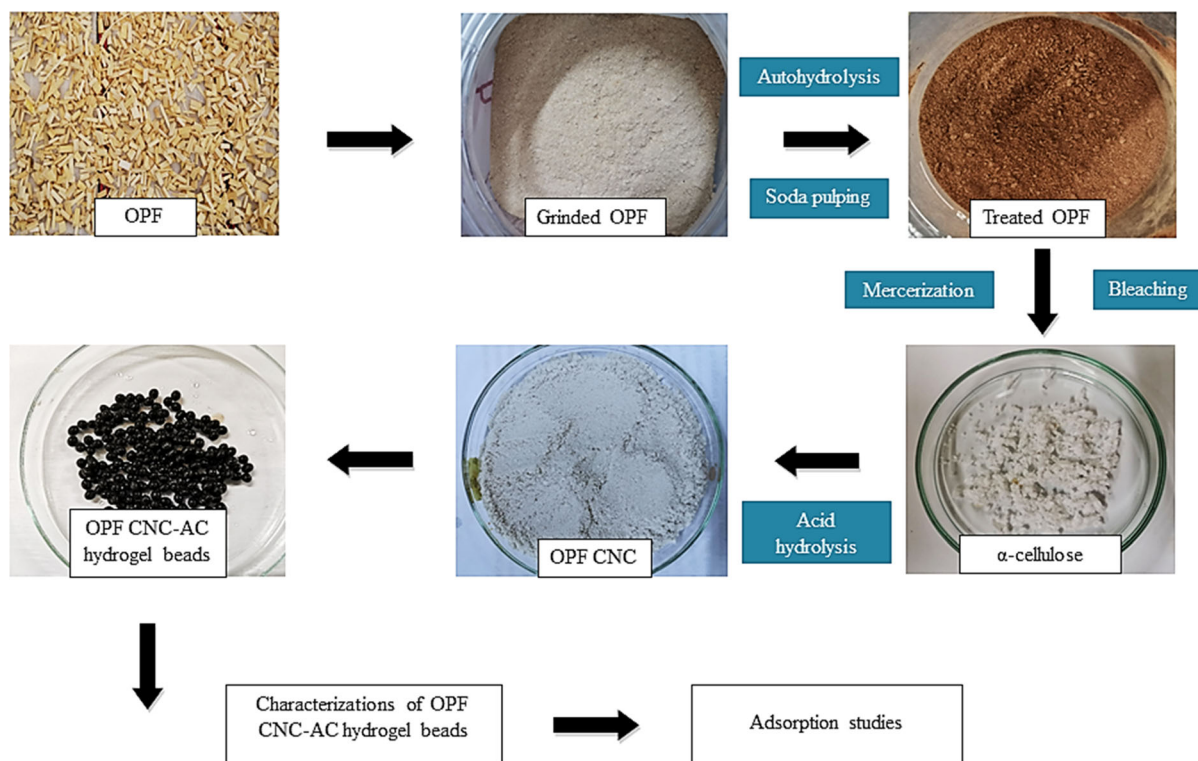
**Fig. 2** The experimental flow diagram

Nanocellulose is a sustainable material, and it has drawn much attention due to its extraordinary properties for various applications (Phanthong et al. 2018). Generally, the term 'nanocellulose' applies to cellulose materials with at least one-nanometer diameter (Blanco et al. 2018). These single cellulose nanometer-sized crystals, commonly called nanowhiskers or nanocrystals, can be produced from different sources (Phanthong et al. 2018). Due to their extraordinary properties for various applications, these nanomaterials have increased in popularity. Recently, the nanoscale science and engineering developments indicate that many of the existing water quality issues can be substantially minimized using nanocellulose extracted from the biomass by dint of their strong adsorption performance, higher surface area, and more significant pollutant interaction active sites (Trache et al. 2020). Besides, AC is a flexible adsorbent utilized in various applications, such as environmental, industrial, and other industries, to eliminate, recover, separate, and modify a wide range of species in liquid and gas-phase applications with a large surface area and high porosity (Çeçen 2014).

However, the practicality of separating nanocellulose from wastewater after adsorption should be dealt with pertinently. To the best of our knowledge, no research studies have been performed on exploiting low-cost OPF CNC-AC hydrogel beads as a potential adsorbent for paracetamol removal in aqueous solutions. Thus, the present research work made an effort to tackle this challenge by incorporating cellulose nanocrystals and AC into alginate hydrogel beads to ease separation upon batch adsorption. In addition, alginate-based hydrogel beads' integral porous structure could improve its retention capacity (i.e. high adsorption capacity) and reusability. The current study presents the data obtained using OPF CNC-AC hydrogel beads to retain paracetamol from aqueous media and their recyclability. The prospective of utilizing sustainable and viable nanomaterials in eliminating pharmaceuticals from waterbodies would garner immense influence for the countries where water pollution has become a foremost environmental concern.

## Experimental

### Materials

The chemicals used in this study are glacial acetic acid, HOAc (QRёC, Malaysia), sulphuric acid, $H_2SO_4$ (97%, QRёC, Malaysia), sodium hydroxide pellets, NaOH (QRёC, Malaysia), sodium chlorite, $NaClO_2$ (Sigma-Aldrich, United States), sodium alginate, $C_6H_7NaO_6$ (Sigma-Aldrich, United States), calcium chloride, $CaCl_2$ (Bendosen, UK), commercial activated carbon (QRёC, Malaysia) and paracetamol (99%, Sigma-Aldrich, United States).

### Cellulose nanocrystals (CNC) preparation

OPF was collected from Kuala Krai, Kelantan, Malaysia, in 2019. The samples were cut into $1 \times 1$ cm size (length $\times$ width) pieces, sun-dried, grounded into powder, and sieved into 250 μm. Then, OPF powder was subjected to autohydrolysis, soda pulping, pulp bleaching, and mercerization processes to obtain pure cellulose, as shown in Fig. 2. The autohydrolysis was carried out utilizing a 0.3 L steel reactor. The steel reactor was loaded with 20 g of dry powdered OPF and mixed with 160 mL of distilled water. The reactor was airtight and heated to 180 °C for 330 min. The reactor was cooled after thermal heating, and the OPF pulp was filtered using Whatman No. 1 filter paper, washed with distilled water, and subsequently dried in a 50 °C oven for 24 h. For the soda pulping process, the conditions used were maintaining the process at the ratio of 1:8 (OPF: water) with 20% active alkaline and 30% sulfidity. The pressure was set at a range of 12–15 bar. The process was conducted for 3 h at 170 °C. Then, the OPF pulp was filtered, rinsed with distilled water, and dried in the oven at 50 °C for 24 h. The pulp bleaching process was carried out by weighing 1.5 g of soda pulp and placing it in a round bottom flask with 125 mL of distilled water. After that, 1 mL of glacial acetic acid and 1 g of sodium chlorite were incorporated. With continuous stirring, the mixture was refluxed for 2 h at 70 °C. The holocellulose was then vacuum filtered and washed with excess distilled water after being refluxed. Finally, the holocellulose was dried for 24 h at 50 °C in an oven. Meanwhile, 2 g of dried holocellulose sample was utilized with 100 mL of 10% (w/v) NaOH for 30 min at room temperature

($27 \pm 1$ °C) for the mercerization process. After 30 min, 100 mL of distilled water was added to the mixture, then stirred continuously at room temperature for another 30 min. The resulting cellulose was then vacuum filtered before being washed with 1% (w/v) glacial acetic acid, 5% (w/v) NaOH, and excess distilled water. Then, the cellulose was then dried for 24 h at 50 °C in an oven. Next, the acid hydrolysis method was conducted to prepare cellulose nanocrystals (Trache et al. 2017). 2.0 g of cellulose was treated with 17.5 mL of 50% (v/v) $H_2SO_4$ for 30 min at room temperature under continuous stirring. After that, the hydrolysis process was stopped by adding cold distilled water. The resulted solution was centrifuged at 7900 rpm for 10 min (4 times). The dialysis process was carried out until pH was neutralized (attaining pH 7), and finally, the CNC samples were freeze-dried at −48 °C for 72 h.

### Synthesis of OPF CNC-AC hydrogel beads

0.2 M $CaCl_2$ solution was prepared by mixing 1.15 g of $CaCl_2$ and 50 mL of distilled water in a 100 mL beaker. The mixed solution was stirred until it was completely dissolved. In order to prepare OPF CNC-AC hydrogel beads, sodium alginate (SA) solution was initially prepared by weighing 400 mg of SA dissolved in distilled water. The solution was stirred until it became viscous and transparent. Then, 200 mg of OPF-CNC powder was added and stirred until it was completely dissolved. Next, 200 mg of commercial AC was added under vigorous stirring until a blackish and well-dissolved solution was formed. The resulting solution was added dropwise into the $CaCl_2$ solution using a dropper to form OPF CNC-AC hydrogel beads. The beads were gently stirred for 30 min to harden the beads and keep the beads from sticking to one another. After stirring, the beads were left in the $CaCl_2$ solution for 24 h to ensure complete gelation and the formation of stable beads. Before carrying out adsorption studies, the beads were rinsed several times with distilled water to remove residual $CaCl_2$ from the surface of the beads and kept in the distilled water for further use.

### Characterization

The main functional groups of OPF CNC-AC hydrogel beads were identified by performing an attenuated
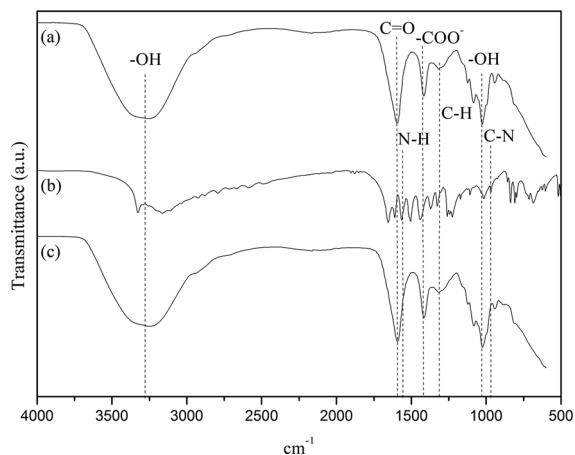
**Fig. 3** FTIR spectra of **a** OPF CNC-AC hydrogel beads before adsorption, **b** paracetamol, and **c** OPF CNC-AC hydrogel beads after adsorption

total reflection (ATR) analysis via Fourier-transform infrared spectrometer (Model Perkin Elmer Frontier FT-IR/NIR). A hydrogel bead was placed on the metal plate for analysis. The spectra analyses were conducted in the range of 4000 cm$^{-1}$ to 400 cm$^{-1}$ with a resolution of 4.0 cm$^{-1}$, and the samples were scanned 20 times. The BET surface area, total pore volume and pore size of OPF-CNC, alginate (ALG) hydrogel beads, and OPF CNC-AC hydrogel beads were analyzed adopting the Brunauer–Emmett–Teller (BET) equation and Quantachrome NovaWin2© software. The surface morphology study was investigated using scanning electron microscopy (SEM). A small quantity of OPF CNC-AC hydrogel beads was placed on a carbon stud and coated by platinum (Pt). The SEM analysis was carried out on a QUANTA FEI 650 at 200 × magnification.

Adsorption studies

The OPF CNC-AC hydrogel beads were put inside the conical flask of 10 mg L$^{-1}$ paracetamol solution (100 mL). The conical flasks were fully covered by aluminium foil to avoid light exposure during the experiment, and the flasks were placed on an orbital shaker (150 rpm, 170 min). Then, the sample solutions were filtered using gravity filtration, and the concentration of filtrate was measured using a UV–Vis spectrophotometer (Shimadzu 2600) at $\lambda$ = 243 nm. Finally, the removal percentage of paracetamol was calculated using the equation below:

$$Paracetamol\ uptake = \left(\frac{C_o - C_e}{C_o}\right) \times 100 \qquad (1)$$

The amount of paracetamol adsorbed at equilibrium, $q_e$ (mg g$^{-1}$), was calculated using the equation below:

$$q_e = \left[\frac{(C_o - C_e)V}{m}\right] \qquad (2)$$

where $C_o$ is the initial paracetamol concentration (mg L$^{-1}$), $C_e$ is the paracetamol concentration at equilibrium (mg L$^{-1}$), V is the volume of paracetamol solution used (L), and m is the mass of adsorbent used (g).

The effects of pH (1–11), contact time (10–170 min), and initial paracetamol concentration (1–1000 mg L$^{-1}$) were investigated. All the experiments were carried out in triplicates under identical conditions, and the average results were reported.

Reusability study

The reusability analysis was carried out with an optimized condition of 0.6 g of adsorbent dosage, 100 mL of 10 mg L$^{-1}$ of paracetamol solution at pH 3 (paracetamol solution were adjusted using 0.1 M HCl and 0.1 M NaOH), shaken in an orbital shaker (150 rpm, 170 min) at a room temperature. Then, the samples were removed from paracetamol solution through gravity filtration, and the filtrate was analyzed by a UV–Vis spectrophotometer at $\lambda$ = 243 nm. The adsorbed samples were desorbed with 5% of ethanol under constant stirring for 6 h. The process of adsorption and desorption were repeated for five cycles.

**Results and discussion**

Characterization of hydrogel beads

*FTIR analysis*

The molecular structure and functional groups of an adsorbent influence its adsorption ability (Yadav et al. 2020). Thus, FTIR analysis was carried out to determine the functional groups of paracetamol and OPF CNC-AC hydrogel beads before and after the adsorption process. Figure 3 illustrates the FTIR

**Table 1** Surface and porosity parameters of OPF-CNC, ALG hydrogel beads, and OPF CNC-AC hydrogel beads obtained from BET analysis

| Samples | BET surface area ($m^2\ g^{-1}$) | Cumulative pore volume ($cm^3\ g^{-1}$) | Average pore width (nm) |
| --- | --- | --- | --- |
| OPF-CNC | 10.51 | 0.0067 | 2.5365 |
| ALG hydrogel beads | 0.91 | 0.0003 | 1.2481 |
| OPF CNC-AC hydrogel beads | 85.19 | 0.0417 | 1.9597 |

spectrum of OPF CNC-AC hydrogel beads, which shows hydroxyl, carbonyl, and carboxyl groups as the main functional groups.

The FTIR spectrum of OPF CNC-AC hydrogel beads before adsorption was highly comparable to that after adsorption. Nevertheless, several peaks had higher intensities and were slightly shifted than those before adsorption. As observed, all spectra except spectra (b) showed a broad absorption band at 3200 to 3400 $cm^{-1}$ which was due to the stretching and bending of -OH groups in the OPF CNC-AC hydrogel beads before and after adsorption. Joshi and Pokharel (2013) stated that the intermolecular hydrogen bonding of alcohols, phenols, and carboxylic acids caused the -OH stretching vibration on the surface of the adsorbent. Therefore, this confirmed free hydroxyl groups on the adsorbent surface (Nche et al. 2017).

In addition, a peak was identified at 1618 $cm^{-1}$ in OPF CNC-AC hydrogel beads corresponding to the stretching vibration of the C = O group (Nasrullah et al. 2018). The peak at 1415 $cm^{-1}$ represents the symmetric carboxylate -$COO^-$ group stretching of SA. This peak confirmed the complex formation of the beads after crosslinking with $Ca^{2+}$ ions (Kumar et al. 2017). Then, a peak was further noticed at 1024 to 1036 $cm^{-1}$ related to the -OH group (Hassan et al. 2014). It could be noticed that after paracetamol adsorption, the intensity of this peak was significantly increased. Also, OPF CNC-AC hydrogel beads showed a peak at 1385 $cm^{-1}$ due to the = C-H stretching of aromatic and asymmetric aliphatic alkyl groups, including –$CH_2$ and –$CH_3$ (Joshi and Pokharel 2013). The peak's strength increased after OPF CNC-AC hydrogel beads were modified with the commercial AC, and as could be noticed, the peaks were broader and more intense. This could suggest that the hydrogel beads have been successfully modified.

Meanwhile, Fig. 3 also shows the FTIR spectrum of OPF CNC-AC hydrogel beads following the

adsorption procedure, which was used to prove the presence of paracetamol on the adsorbent surface. For the paracetamol spectrum, there was a presence of a peak at 1565 $cm^{-1}$ due to the N–H amide II bending, while the absorption peak of C-N (amide) stretching appeared at 965 $cm^{-1}$. Paracetamol was found to have the vibrational peak of O–H stretching at 3326 $cm^{-1}$ (Trivedi et al. 2015). However, the peak was not as broad as the O–H stretching for OPF CNC-AC hydrogel beads. As observed, a higher intensity of adsorption peaks was noticed at 1590 to 1618 $cm^{-1}$ and 1024 to 1036 $cm^{-1}$ after the adsorption process. The increase in the intensity of the peak was due to the interaction of paracetamol molecules and OPF CNC-AC hydrogel beads as the paracetamol molecules interact with the beads via electrostatic interactions.

*BET analysis*

The surface area of the substance was determined by using the Brunauer–Emmett–Teller (BET) technique. The BET surface area, cumulative pore volume and average pore width of OPF-CNC, ALG hydrogel beads, and OPF CNC-AC hydrogel beads were listed in Table 1. According to the table, the value of BET surface area, cumulative pore volume, and average pore width of OPF CNC-AC hydrogel beads was higher than OPF-CNC and ALG hydrogel beads. Besides, it could be noticed that the modification of OPF CNC-AC hydrogel beads using commercial AC improved the beads' surface area, pore volume, and pore width, which resulted in the structure having a more significant pore. Therefore, the highest value of the specific surface area and cumulative pore volume correspond to the OPF CNC-AC hydrogel beads with 85.19 $m^2\ g^{-1}$ and 0.0417 $cm^3\ g^{-1}$, while the lowest corresponds to the ALG hydrogel beads with 0.91 $m^2\ g^{-1}$ and 0.0003 $cm^3\ g^{-1}$.

According to the International Union of Pure and Applied Chemistry (IUPAC), pores are categorized as micropores (< 2 nm in diameter), mesopores (2–50 nm in diameter), and macropores (> 50 nm in diameter) (Everett 1972). The OPF-CNC can be classified as mesopores, while the ALG hydrogel beads and OPF CNC-AC hydrogel beads can be classified as micropores based on the average pore width, which indicated that the porosity structure was good. Thus, the paracetamol molecules can easily penetrate the beads due to their porous structure. This can be seen through the presence of the N element in the cross-section of OPF CNC-AC hydrogel beads after the adsorption of paracetamol. This proved that the paracetamol encountered not just the surface of the hydrogel beads but also within the cross-section of the beads. Consequently, it seems that OPF CNC-AC hydrogel beads can remove paracetamol from the wastewater.

*SEM analysis*

The SEM micrographs for surface morphology and cross-section of ALG and OPF CNC-AC hydrogel beads (before and after adsorption) are shown in Fig. 4. All samples displayed a wrinkled morphology. For ALG hydrogel beads, the cross-section showed a smoother surface compared to OPF CNC-AC hydrogel beads. As observed, the surface of the beads changed from smooth to rougher when CNC was added (Supramaniam et al. 2018). CNC added further undulations and folds to the surface of the beads, thereby expanding the surface area and increasing the binding sites available for the adsorption studies (Mohammed et al. 2015). Besides, the surface of OPF CNC-AC hydrogel beads was rough and uneven with irregular pores. The cross-sectional image clearly showed that the modified beads exhibit several pores of various shapes and sizes and have a highly interconnected irregular large space (cavities) (Nasrullah et al. 2018). Therefore, this loose arrangement and surface pores facilitate molecular diffusion and supply enough free space for molecules, enabling paracetamol adsorption. Many contaminants can be adsorbed by the porous beads, which have a high surface area. Javadian et al. (2015) stated that the adsorbent's surface area is directly proportional to the adsorption efficiency. The higher the surface area, the higher the adsorption efficiency. Meanwhile, after

**Fig. 4** SEM images of **a** cross-section of ALG hydrogel bead, ▶ **b** and **d** surface morphology of OPF CNC-AC hydrogel beads (before and after adsorption), **c**, and **e** cross-section of OPF CNC-AC hydrogel beads (before and after adsorption) at 200 × magnification

adsorption, the paracetamol molecules fill most of the available pores within the OPF CNC-AC hydrogel beads. Therefore, the surface of cross-sectional OPF CNC-AC hydrogel beads became saturated compared to before adsorption.

Effect of various parameters influencing paracetamol adsorption

*Effect of pH*

Figure 5 illustrates the effect of pH on percentage removal and adsorption capacity ($q_e$) of paracetamol by OPF CNC-AC hydrogel beads. The effect of pH on paracetamol adsorption was investigated between pH 1 and 11. Mohd et al. (2015) reported that pH variations impact the adsorbent's surface chemistry due to the dissolution of functional groups. The figure shows that as paracetamol solution became more basic, the percentage removal was decreased. The highest percentage removal was at pH 3 with $79.98 \pm 0.58\%$ and adsorption capacity, $q_e$ of $1.33 \pm 0.01$ mg g$^{-1}$ while the lowest was at pH 1 with $51.19 \pm 0.30\%$ and $q_e$ of $0.85 \pm 0.01$ mg g$^{-1}$. At pH 1, the size of the beads reduced and became smaller as the paracetamol solution was too acidic. Thus, the beads' efficiency was also reduced, resulting in the lowest percentage removal of paracetamol.

At an acidic solution with a pH value between pH 2 and 4, paracetamol exists in its neutral state. However, the negative charge of activated carbon neutralized most all the negatively charged surface with hydrochloric acid (Mohd et al. 2015). Hence, the repulsion between the neutral adsorbent molecule and the positively charged AC surface was considerably reduced and advocated an effective paracetamol removal. Ferreira et al. (2015) stated that an effective paracetamol removal might be due to the highest electronic charges of neutral paracetamol molecule found in the C = O group that could be attracted to the positively charged adsorbent's surface.
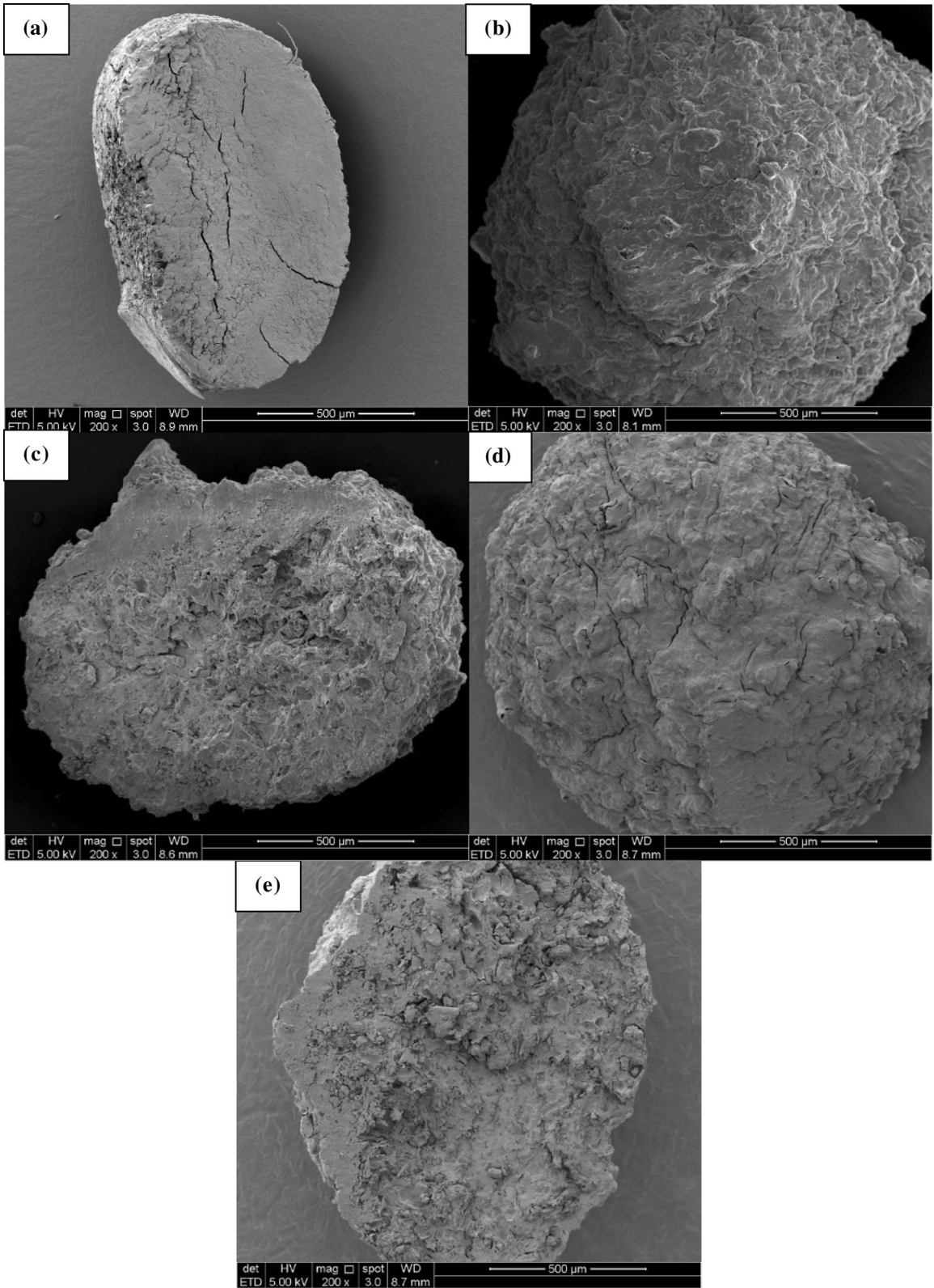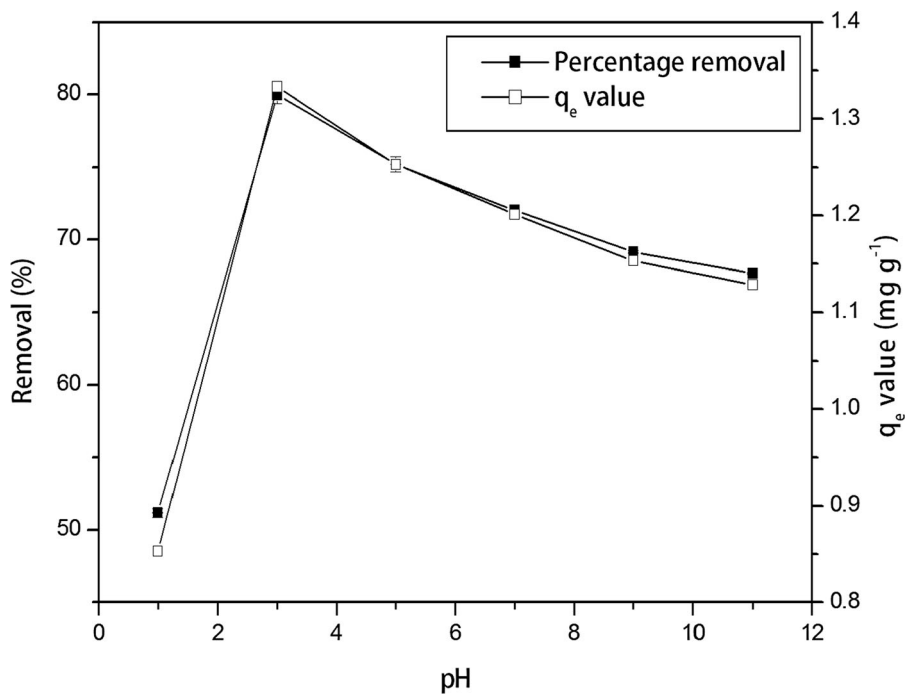
**Fig. 5** Percentage removal and effect of pH on paracetamol by OPF CNC-AC hydrogel beads at 27 ± 1 °C
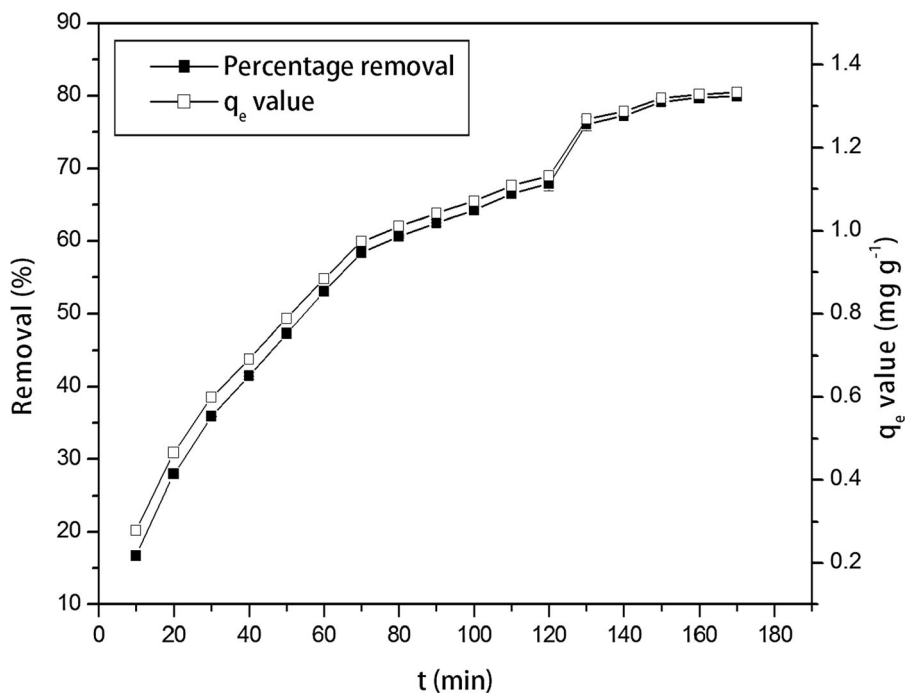


**Fig. 6** Percentage removal and effect of contact time on paracetamol by OPF CNC-AC hydrogel beads at 27 ± 1 °C
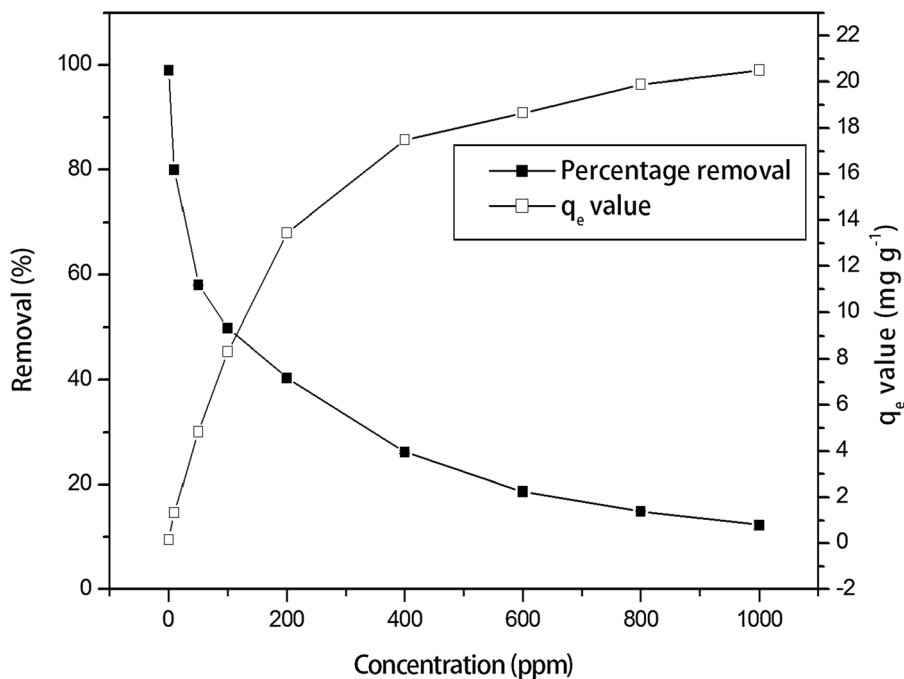
**Fig. 7** Percentage removal and effect of initial paracetamol concentration by OPF CNC-AC hydrogel beads at $27 \pm 1$ °C

Meanwhile, in a basic solution, the loading capacities were decreased, which could be attributed to two aspects; adsorbate ionization and the charges surface of AC at that pH (Sikarwar and Jain 2014). According to the earlier studies, the surface of the AC is negatively charged. Thus, both adsorbent and adsorbate have a negative-negative charge that repels toward each other, and this clarified why the percentage removal of paracetamol was reduced in a basic solution (Mohd et al. 2015). Besides, the other reason was due to the anionic charges involved in basic solutions where pH greater than pKa (Ferreira et al. 2015). As previously stated, the pKa value of paracetamol is around 9.38 (Mashayekh-Salehi and Moussavi 2016). Paracetamol often exists as a neutral molecule at pH 2, but as it gets closer to its pKa, about half of it ionizes and becomes an anionic molecule. It was reported that paracetamol molecules have a higher density charge in basic solutions and the negatively charged solid sample repelled this charge. Based on the findings, the optimum pH of OPF CNC-AC hydrogel beads was found to be at pH 3.

*Effect of contact time*

The relationship between contact time, $q_e$, and percentage removal of paracetamol by OPF CNC-AC hydrogel beads is shown in Fig. 6. The effect of contact time was studied, ranging from 10 to 170 min to find the minimum time for OPF CNC-AC hydrogel beads to adsorb 10 mg L$^{-1}$ of paracetamol. It was noted that as contact time increased, there was an increase in the percentage removal as well as the $q_e$ until the equilibrium was attained. As could be seen in the figure, the highest percentage removal of paracetamol was observed at 170 min with $79.98 \pm 0.21\%$ and $q_e$ value of $1.33 \pm 0.004$ mg g$^{-1}$.

Meanwhile, in the first 70 min, both the percentage removal and $q_e$ increased sharply and then further increased, reaching a nearly constat equilibrium at 130 min. The $q_e$ values of paracetamol adsorbed by OPF CNC-AC hydrogel beads rose from 0.279 to 1.333 mg g$^{-1}$, increasing contact time from 10 to 170 min. Because of enough adsorption sites on the adsorbents, paracetamol was readily adsorbed at the initial stage. According to Yamuna and Namasivayam (1993), this trend might be described because many unoccupied active sites were available for adsorption at an early stage. However, the excess unoccupied

sites were challenging to occupy after a certain period because of the repulsive forces between solute molecules on solid and bulk phases.

### Effect of initial paracetamol concentration

Figure 7 illustrates the $q_e$ and the effect of initial paracetamol concentration on the amount of paracetamol adsorbed. The amount of paracetamol adsorbed was greatly influenced by the initial concentration. The percentage removal decreased, and the $q_e$ increased as the initial concentration of paracetamol increased due to the concentration gradient's increasing driving force (Hu et al. 2018). Based on the figure, the highest percentage removal of paracetamol onto OPF CNC-AC hydrogel beads was found at 1 mg $L^{-1}$ with 99.00%, while the lowest was at 1000 mg $L^{-1}$ with 12.30 ± 0.56%.

In addition, the $q_e$ of paracetamol increased with an increasing initial concentration of paracetamol from 0.165 to 20.51 ± 0.93 mg $g^{-1}$. Tsai et al. (2009) stated that this could be ascribed to the higher mass transfer of paracetamol molecules to the given mass of adsorbent. The existence of more adsorption sites on the AC than the solute molecules in solution may result in an increased adsorption rate at lower paracetamol concentration (Mukoko 2016). At the same time, a lower adsorption rate was observed at a higher paracetamol concentration. This is because the number of paracetamol molecules is elevated at a greater concentration level than the number of adsorption sites available. Furthermore, the paracetamol molecules aggregate at a higher concentration, generating a slow adsorption process. Mashayekh-Salehi and Moussavi (2016) reported a similar finding in their analysis of dried pomegranate wood's ability to remove paracetamol from aqueous solutions.
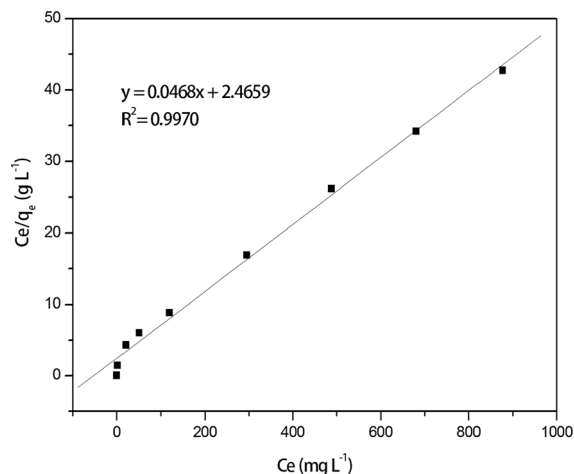


**Fig. 8** Langmuir-1 isotherm plot of paracetamol adsorption onto OPF CNC-AC hydrogel beads at 27 ± 1 °C

### Adsorption isotherms

Adsorption isotherm models are commonly used to determine the maximum retention capacity and describe the processes and mechanism of adsorption (Ferchichi and Dhaouadi 2016; Yadav et al. 2020). Various equilibrium isotherms have been suggested with different models to describe the adsorption procedure, such as Langmuir, Freundlich, Temkin, and Dubinin-Radushkevich. The models demonstrate the relationship between the quantity of adsorbent adsorbed and the adsorbate concentration that remained in the medium at equilibrium (Mohd et al. 2015).

### Langmuir isotherm

Langmuir isotherm is first defined by Langmuir (1918). It is modelled on the assumption that monolayer adsorption occurs at homogeneous sites and adsorbent surfaces, with no additional adsorption occurring at sites of adsorption once they have been occupied. The Langmuir equation is given as:

| Table 2 Langmuir parameters of OPF CNC-AC hydrogel beads by linear regression method | Linear Langmuir isotherms | $K_L$ (L $g^{-1}$) | $a_L$ (L $mg^{-1}$) | $q_{max}$ (mg $g^{-1}$) | $R^2$ |
|---|---|---|---|---|---|
| | Langmuir-1 | 0.4055 | 0.0190 | 21.3420 | 0.9970 |
| | Langmuir-2 | 16.9492 | 2.8051 | 6.0423 | 0.9940 |
| | Langmuir-3 | 16.0101 | 1.2067 | 13.2677 | 0.5555 |
| | Langmuir-4 | 6.3093 | 0.3723 | 16.9468 | 0.5555 |

**Table 3** Comparison of monolayer adsorption capacities of paracetamol on different adsorbents

| Adsorbent | Maximum adsorption capacity (mg g$^{-1}$) | Initial concentration of paracetamol (mg/L) | Solution pH | Contact time (h) | Solution temperature (°C) | References |
|---|---|---|---|---|---|---|
| Babassu coconut mesocarp AC | 65.29 | 50 | 2.0 | 4.0 | ± 25 | (Ferreira et al. 2015) |
| Spent tea leaves AC | 59.17 | 10 | 3.0 | 1.0 | ± 30 | (Wong et al. 2018) |
| Commercial AC | 25.25 | 100 | 2.0 | 2.0 | 40 | (Mohd et al. 2015) |
| OPF CNC-AC hydrogel beads | 21.34 | 10 | 3.0 | 2.8 | ± 27 | Present work |
| Oxidized AC from coconut shell | 16.80 | 1000 | 7.0 | – | ± 25 | (Bernal et al. 2017) |
| Rice husk AC | 14.88 | 100 | 2.0 | 1.7 | ± 27 | (Nche et al. 2017) |
| Primary sludge charcoal | 12.33 | 100 | 6.9 | 72.0 | 25 ± 2 | (Coimbra et al. 2019) |
| Polymeric resin Sepabeads | 8.25 | 100 | – | 3.3 | 25 ± 2 | (Coimbra et al. 2018) |
| P. oceanica | 1.64 | 100 | 5.7 | 24.0 | ± 25 | (Ferchichi and Dhaouadi 2016) |
| Dehydrated sewage sludge | 0.96 | 100 | 5.7 | 24.0 | ± 25 | (Ferchichi and Dhaouadi 2016) |

" – " specifies the relevant information was not stated in the references

$$\frac{C_e}{q_e} = \frac{1}{q_{max}K_L} + \frac{C_e}{q_{max}} \qquad (3)$$

where $q_e$ is the adsorbate amount adsorbed per unit adsorbent weight (mg g$^{-1}$), $q_m$ is the maximum adsorption capacity (mg g$^{-1}$), $C_e$ is the equilibrium liquid phase concentration (mg L$^{-1}$), $K_L$ and $a_L$ are the Langmuir isotherm constant (L mg$^{-1}$) (Soto et al. 2011). The $q_{max}$ was computed using the equation below (Goel et al. 2015):

$$q_{max} = \left(\frac{K_L}{a_L}\right) \qquad (4)$$

Additionally, the Langmuir isotherm model could be transformed into four distinct forms of linear expressions (Goel et al. 2015).

$$Langmuir - 1 : \frac{C_e}{q_e} = \left(\frac{1}{K_L}\right) + \left(\frac{a_L}{K_L}\right)C_e \qquad (5)$$

$$Langmuir - 2 : \frac{1}{q_e} = \left(\frac{a_L}{K_L}\right) + \left(\frac{1}{K_L}\right)\left(\frac{1}{C_e}\right) \qquad (6)$$

$$Langmuir - 3 : q_e = \left(\frac{K_L}{a_L}\right) - \left(\frac{1}{a_L}\right)\left(\frac{q_e}{C_e}\right) \qquad (7)$$

$$Langmuir - 4 : \frac{q_e}{C_e} = K_L - a_L q_e \qquad (8)$$

A dimensionless constant separation factor ($R_L$) may show the fundamental characteristics of a Langmuir isotherm (Chuein et al. 2021; Langmuir 1918):

$$R_L = \frac{1}{1 + K_L C_o} \qquad (9)$$

where $C_o$ is the initial concentration (mg L$^{-1}$), while the type of isotherm could be indicated by the value of $R_L$.

$R_L$ value indicates the adsorption to be either irreversible adsorption ($R_L = 0$), favourable adsorption ($0 < R_L < 1$), linear adsorption ($R_L = 1$), or unfavourable adsorption ($R_L > 1$) (Hamad et al. 2010). Table 2 summarizes the relevant parameters from linear Langmuir isotherms, and Fig. 8 shows the Langmuir-1 isotherm plot of paracetamol adsorption on OPF CNC-AC hydrogel beads.

The Langmuir parameter, $a_L$ and the maximum monolayer adsorption capacity, $q_{max}$ for Langmuir-1 was 0.019 L mg$^{-1}$ and 21.342 mg g$^{-1}$, respectively. Goel et al. (2015) reported that as the value of $a_L$ increases, the adsorption process on the adsorbent becomes greater. The calculated $R_L$ values were in the

range of 0.0500–0.9814, which has been depicted in Fig. S1. However, the value was still within the range $0 < R_L < 1$, which indicated that the nature of the adsorption mechanism was favourable.

In addition, the Langmuir-1 isotherm model displayed the best fit for the adsorption of paracetamol onto OPF CNC-AC hydrogel beads with the highest $R^2$ value of 0.9970. Thus, this demonstrates paracetamol's monolayer adsorption onto OPF CNC-AC hydrogel beads, and the Langmuir-1 isotherm model more suitably describes this adsorption process. Similar findings were reported in rice hull (Mukoko 2016), Neptune grass, and dehydrated sewage sludge (Ferchichi and Dhaouadi 2016), proving that paracetamol adsorption occurred on homogeneous sites. The comparison of $q_{max}$ of paracetamol adsorption pertaining to various adsorbents is summarized in Table 3. The comparative analysis with other adsorbents revealed that OPF CNC-AC hydrogel beads employed in this study have higher adsorption capacity than most of the other adsorbents, which could be due to the availability of high concentration of adsorption sites and the porosity of alginate-based hydrogel beads. According to Blanco et al. (2018), nanocelluloses are utilized as a novel type of biobased adsorbent that is particularly effective for environmental clean-up. This is because nanocelluloses have excellent mechanical properties and can attach practically any desired functional group

due to their large surface area, ability to hold a significant amount of water, and the reactive surface of side groups of -OH (Habibi 2014).

Apart from that, the Langmuir-1 isotherm model can be used to calculate the Gibbs free energy of adsorption ($\Delta G$) to determine whether an adsorption process favours chemisorption or physisorption (Raghav and Kumar 2018). For example, Gibbs free energy could be calculated using the equation below (Mouni et al. 2018):

$$\Delta G = -RT \, lnK_L \tag{10}$$

where R is the universal gas constant (8.314 J K$^{-1}$ mol$^{-1}$), T is the temperature (K), and $K_L$ is the Langmuir isotherm constant.

Suppose the value of $\Delta G$ is around -20 kJ mol$^{-1}$ or less negative. In that case, the adsorption process follows the physisorption mechanism, whereas if the $\Delta G$ is around -40 kJ mol$^{-1}$ or more negative, the adsorption process follows the chemisorption mechanism (Tan et al. 2018). In this study, $\Delta G$ was found to be -10.27 kJ mol$^{-1}$. Thus, as indicated by the negative value of $\Delta G$, it was proven that the surface of OPF CNC-AC hydrogel beads physically and spontaneously adsorbed paracetamol molecules.

**Table 4** Isotherm parameters values of paracetamol adsorption onto OPF CNC-AC hydrogel beads at $27 \pm 1$ °C

| Model | Parameters | Temperature at $27 \pm 1$ °C |
|---|---|---|
| Langmuir | $q_{max}$ (mg g$^{-1}$) | 21.3420 |
| | $K_L$ (L g$^{-1}$) | 0.4055 |
| | a (L mg$^{-1}$) | 0.0190 |
| | $R_L$ | 0.0500–0.9814 |
| | $R^2$ | 0.9970 |
| | $\Delta G$ (kJ mol$^{-1}$) | −10.2654 |
| Freundlich | $K_F$ (mg g$^{-1}$) | 1.2395 |
| | n | 2.2538 |
| | $R^2$ | 0.9947 |
| Temkin | $B_T$ (L mg$^{-1}$) | 1.9737 |
| | $K_T$ | 9.2378 |
| | $\Delta H_T$ (kJ mol$^{-1}$) | −1.2637 |
| | $R^2$ | 0.8890 |
| Dubinin-Radushkevich | $q_{max}$ (mg g$^{-1}$) | 10.0072 |
| | $\beta$ (mol$^2$ kJ$^{-2}$) | 0.0310 |
| | $E_a$ (kJ mol$^{-1}$) | 4.0161 |
| | $R^2$ | 0.8402 |

## Freundlich isotherm

Freundlich model demonstrates that adsorbate molecules form multilayers on the adsorbent surface during heterogeneous adsorption, and the interactions between adsorbate molecules are not negligible (Wong et al. 2018). According to Haitham et al. (2019), this model allows for reversible adsorption and is not limited to monolayer formation. Freundlich isotherm model can be expressed into the equation below (Freundlich 1906):

$$lnq_e = lnK_F + \frac{1}{n}lnC_e \quad (11)$$

where $C_e$ is the equilibrium liquid phase concentration (mg L$^{-1}$), $q_e$ is the adsorption capacity at equilibrium (mg g$^{-1}$), $K_F$ is the Freundlich isotherm constant (L mg$^{-1}$), and 1/n is the heterogeneity factor; n is the constant for intensity.

The intercept and slope of the Freundlich plot are used to derive the values of $K_F$ and n. Oladipo et al. (2014) stated that if the value of n is between $1 < n < 10$, it is referred to as favourable adsorption, whereas $n > 10$ is attributed to more vigorous adsorption intensity.

The Freundlich linear plot's $R^2$ was discovered to be 0.9947. The values of $K_F$ and n were 1.2395 and 2.2538, respectively, indicating that the adsorption of paracetamol onto OPF CNC-AC hydrogel beads was favourable. Mukoko (2016) reported that if n is between 2 and 10, thus it suggests good adsorption. Besides, a greater n value represents the paracetamol molecules, and OPF CNC-AC hydrogel beads create a stronger connection. Table 4 summarizes the isotherm parameters values, and the linearized plot of Freundlich isotherm is shown in Fig. S2.

## Temkin isotherm

Temkin isotherm model defined the effects of indirect adsorbate–adsorbate interactions (Dada et al. 2012). According to this model, the biosorption heat of molecules on the layer decreases linearly rather than logarithmically as coverage increases. The Temkin equation is given as (Martins et al. 2015):

$$q_e = B_TlnK_T + B_TlnC_e \quad (12)$$

where $K_T$ refers to the Temkin isotherm equilibrium binding constant, $B_T$ is the Temkin isotherm constant associated with adsorbate–adsorbate interaction and adsorption heat $\Delta H_T$ can be found using the following Eq. 13.

$$B_T = \frac{-RT}{\Delta H_T} \quad (13)$$

with R is the universal gas constant of 8.314 J mol$^{-1}$ K$^{-1}$ and T is the temperature (K) (Olgun and Atar 2009).

The adsorption heat, $\Delta H_T$, is vital in determining if the adsorbent acts as physisorption or chemisorption. Table 4 shows the Temkin constant, $B_T$ and $K_T$ computed from the qe vs ln Ce plot in Fig. S3. As seen in the table, physisorption was the primary adsorption process since the calculated $\Delta H_T$ value was seen to be $-1.2637$ kJ mol$^{-1}$, greater than $-20$ kJ mol$^{-1}$ (Tan et al. 2018). Besides, the equilibrium data of paracetamol adsorption onto OPF CNC-AC hydrogel beads did not fit well since the $R^2$ value, 0.8890, was lower than the correlation coefficient obtained for the Langmuir isotherm model.

## Dubinin-Raduskevich isotherm

Dubinin-Radushkevich isotherm model may be used to calculate the adsorbent's maximum adsorption capacity and the adsorption energy per unit of the adsorbate (Luo et al. 2016). Rieman and Walton (2013) reported that the physical or chemical adsorption process was determined by the value of sorption energy, $E_a$. The Dubinin-Raduskevich isotherm constant was calculated using the following formula (Dubinin et al. 1947).

$$lnq_e = lnq_{max} - \beta\mathcal{E}^2 \quad (14)$$

where β is the constant of Dubinin-Radushkevich isotherm associated with adsorption energy (mol$^2$ kJ$^{-2}$), $q_{max}$ is the maximum adsorption capacity (mg g$^{-1}$), and ε represents the Polanyi potential given by:

$$\mathcal{E} = RTln\left(1 + \frac{1}{C_e}\right) \quad (15)$$

The mean free energy adsorption $E_a$ can be identified from the Dubinin-Radushkevich isotherm β, derived in Eq. (15):

$$E_a = \frac{1}{\sqrt{2\beta}} \quad (16)$$

**Table 5** The pseudo-first and pseudo-second order kinetic models for the adsorption of paracetamol onto OPF CNC-AC hydrogel beads

| Initial paracetamol concentration (mg $L^{-1}$) | $q_{e,exp}$ (mg $g^{-1}$) | First-order kinetic model | | | | Second-order kinetic model | | | |
| --- | --- | --- | --- | --- | --- | --- | --- | --- | --- |
| | | $q_{e,cal}$ (mg $g^{-1}$) | $k_1$ ($min^{-1}$) | $R^2$ | $\Delta q_e$ (%) | $q_{e,cal}$ (mg $g^{-1}$) | $k_2$ (g $mg^{-1}$ $min^{-1}$) | $R^2$ | $\Delta q_e$ (%) |
| 10 | 1.3390 | 2.4811 | 0.0292 | 0.9299 | 60.31 | 1.8126 | 0.0089 | 0.9946 | 25.01 |

The adsorption process follows the chemisorption mechanism when the sorption energy value is between 8 and 16 kJ $mol^{-1}$, while the process corresponds to physisorption when the $E_a$ is less than 8 kJ $mol^{-1}$. The Dubinin-Radushkevich isotherm model is portrayed in Fig. S4. As shown in Table 4, the $E_a$ value was 4.0161 kJ $mol^{-1}$, suggesting that the physical adsorption dominates the adsorption of paracetamol onto OPF CNC-AC hydrogel beads. However, the equilibrium data of the adsorption did not match well with the Dubinin-Radushkevich isotherm model. Therefore, all the isotherm models are listed in the given order according to the linear regression correlation coefficient ($R^2$): Langmuir $R^2$ (0.9970) > Freundlich $R^2$ (0.9947) > Temkin $R^2$ (0.8890) > Dubinin-Radushkevich $R^2$ (0.8402).

Thus, when comparing all four isotherm models, it can be concluded that the overall results showed the adsorption process of paracetamol onto OPF CNC-AC hydrogel beads was best described by the Langmuir isotherm model, with an $R^2$ value is near to the unity.

Adsorption kinetics

The kinetics of adsorption is to establish the time course of paracetamol uptake on the CNC-AC hydrogel beads. Several kinetic models have been proposed to investigate the controlling mechanism of adsorbate adsorbed by an adsorbent. Adsorption kinetics are classified into two models; the adsorption diffusion (intra-particle diffusion model) and adsorption reaction models (pseudo-first order, pseudo-second order and Elovich kinetic model), which include mechanism and rate control step details (Oladipo et al. 2014). By combining the adsorption kinetic data with various kinetic models, the rate and mechanism of paracetamol adsorption onto OPF CNC-AC hydrogel beads can be identified. Pseudo-first order model, pseudo-second order model, Elovich model and intraparticle
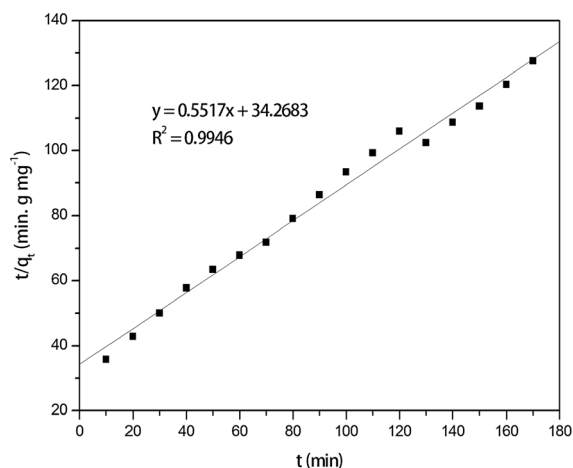


**Fig. 9** Pseudo-second order kinetic model plot for the adsorption of paracetamol onto OPF CNC-AC hydrogel beads at 27 ± 1 °C

diffusion model are the four most commonly used kinetic models. However, only the intraparticle diffusion model describes the diffusion mechanism of an adsorbate. According to Fig. 6, the CNC-AC hydrogel beads' relatively fast initial adsorption rate may probably be due to their three-dimensional structure and possibly due to the relatively large specific surface area, which provided a high density of surface adsorption sites.

*Pseudo-first order*

In general, Lagergren (1898) established a simple kinetic model for predicting the surface adsorption rate, known as pseudo-first order. This model describes a reaction in which the adsorption rate is influenced by the diffusion phase (Hu et al. 2019). For example, the following equation expresses the pseudo-first order equation:

$$log(q_e - q_t) = logq_e - \left(\frac{k_1}{2.303}\right)t \qquad (17)$$

where $q_e$ and $q_t$ is the amount of solute adsorbed per unit weight of adsorbent at equilibrium (mg g$^{-1}$) and at any time (min), while $k_1$ is the pseudo-first-order rate constant for the kinetic model (min$^{-1}$).

$k_1$ and the adsorption amount, $q_{e, cal}$ could be determined using the slope and intercept of log ($q_e - q_t$) versus t (min). The pseudo-first order plot of OPF CNC-AC hydrogel beads is shown in Fig. S5, whereas the values of their corresponding parameters are tabulated in Table 5.

Apart from that, the models' applicability in determining their parameters was assessed using the determination coefficient values ($R^2$) and normalized standard deviation ($\Delta q_e$). The $\Delta q_e$ was determined to aid in selecting the best-fitting model, as it represents the fit between anticipated and experimental adsorption capacity data (Tan et al. 2018). The $\Delta q_e$ (%) values were calculated according to the equation below (Spessato et al. 2019):

$$\Delta q_e(\%) = 100 \times \sqrt{\frac{\sum\left[(q_{e,exp} - q_{e,cal})/q_{e,exp}\right]^2}{N-1}} \qquad (18)$$

where $q_{e,exp}$ and $q_{e,cal}$ refer to the experimental and calculated amounts of the paracetamol adsorbed at equilibrium onto OPF CNC-AC hydrogel beads (mg g$^{-1}$), respectively. Meanwhile, N corresponds to the number of adsorption assays.
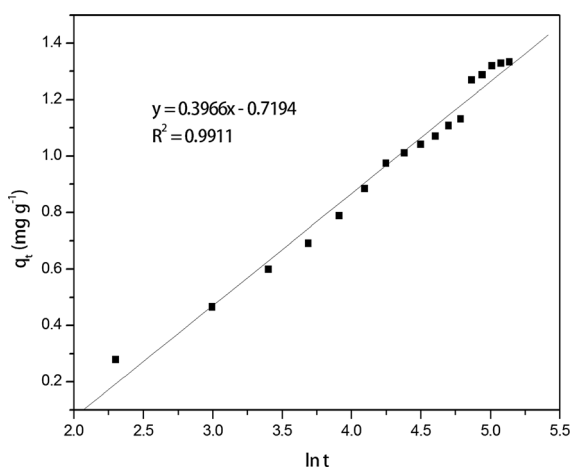
From Table 5, the $R^2$ value of pseudo-first-order, which was 0.9299, was lower than those found in pseudo-second-order, with a much higher normalized standard deviation value of 60.31%. Thus, the adsorption of paracetamol onto OPF CNC-AC hydrogel beads was not compatible with the pseudo-first order model. A similar finding was reported by Mukoko (2016) on the adsorption of paracetamol, ibuprofen, and aspirin.

### Pseudo-second order

The pseudo-second order kinetic model is widely used to study solid to liquid adsorption (Tan et al. 2018). According to Ho and McKay (1998), the rate-limiting step could be chemisorption due to the solution's removal was most likely due to the physical interaction between two phases. The pseudo-second order equation is written as follows:

$$\frac{t}{q_t} = \frac{t}{q_e} + \frac{1}{k_2 q_e^2} \qquad (19)$$

where $k_2$(g mg$^{-1}$ min$^{-1}$) is the pseudo-second order adsorption's rate constant. From the slope and intercept of t/$q_t$ versus t (min) plot, the pseudo-second order rate constant, $k_2$ and $q_e$ could be derived.

Figure 9 shows the pseudo-second order plot for the adsorption of paracetamol by OPF CNC-AC hydrogel beads, while Table 5 shows the value of their corresponding parameters. It was noticed that the pseudo-second order kinetic model showed an
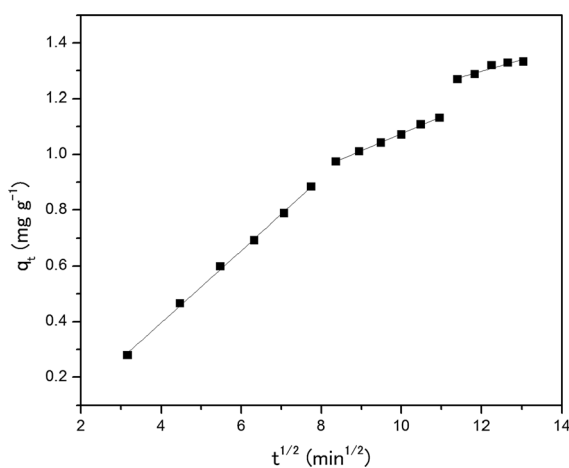


**Fig. 10** Elovich kinetic model plot for the adsorption of paracetamol onto OPF CNC-AC hydrogel beads at 27 ± 1 °C

y = 0.3966x - 0.7194
$R^2$ = 0.9911



**Fig. 11** Intra-particle diffusion model plot for the adsorption of paracetamol onto OPF CNC- AC hydrogel beads at 27 ± 1 °C

**Table 6** The intra-particle diffusion constants and linear regression coefficients at 10 mg L$^{-1}$ paracetamol concentration

| Initial paracetamol concentration (mg L$^{-1}$) | $K_{p,1}$ (mg g$^{-1}$ min$^{-1/2}$) | $R^2$ | $K_{p,2}$ (mg g$^{-1}$ min$^{-1/2}$) | $R^2$ | $K_{p,3}$ (mg g$^{-1}$ min$^{-1/2}$) | $R^2$ |
|---|---|---|---|---|---|---|
| 10 | 0.1297 | 0.9982 | 0.0614 | 0.9980 | 0.0415 | 0.8952 |

excellent fit with an $R^2$ value of 0.9946 and a lower $\Delta q_e$ value of 25.01%. Apart from that, $q_{e,cal}$ obtained from this model agreed well with $q_{e,exp}$, indicating that the pseudo-second order kinetic model better described the adsorption of paracetamol by OPF CNC-AC hydrogel beads. Furthermore, the $q_{e,cal}$ value of 1.8126 mg g$^{-1}$ was relatively comparable with Tan et al. (2018). Similar findings for the adsorption of organic compounds like dyes, herbicides, oils, and organic substances from aqueous solutions also have been successfully utilized using this approach (Ho 2006).

*Elovich kinetic model*

According to the Elovich kinetic model, the chemisorption agrees with the adsorption activity of gases on a solid surface (Tan et al. 2018). The linear equation model is shown below (Chien and Clayton 1980):

$$q_t = \frac{1}{\beta} ln(\beta\alpha) + \frac{1}{\beta} ln(t) \qquad (20)$$

where $\beta$ refers to the constant rate related to coverage surface and activation energy of chemisorption (g mg$^{-1}$) while $\alpha$ represents the initial rate of adsorption (mg g$^{-1}$ min$^{-1}$).

In this model, the values of $\alpha$ and $\beta$ differ as to the initial pharmaceutical concentration function. Therefore, the slope and intercept of the linear plot of $q_t$ versus ln t (Fig. 10) can be used to compute the values of $\alpha$ and $\beta$.

Even though the adsorption of paracetamol onto OPF CNC-AC hydrogel beads was excellently suited in Pseudo-second order, the Elovich kinetic model was the most appropriate equation since it characterized the adsorption behaviour in a way that corresponded to the nature of chemisorption (Tan et al. 2018). As observed, Elovich kinetic model does not offer a good $R^2$, which was 0.9911 with $\alpha$ and $\beta$ values of 0.0647 mg g$^{-1}$ min$^{-1}$ and 2.5214 g mg$^{-1}$,

respectively. As a result, it is possible to explain that the adsorption mechanism of paracetamol onto OPF CNC-AC hydrogel beads did not involve chemisorption. A similar result was obtained by Dutta et al. (2015), who also studied the adsorption of paracetamol by using tea waste-derived AC.

*Intra-particle diffusion*

This model was suggested by Weber Jr and Morris (1963), assuming the adsorption process occurs when adsorbate molecules diffuse or disperse into the adsorbent pores. In comparison to other models, intra-particle diffusion is the best suitable kinetic model for defining the mechanism of diffusion and rate-controlling phases in the adsorption process (Tan et al. 2018). The intra-particle diffusion equation is shown below:

$$q_t = k_{p,i} t^{1/2} + C \qquad (21)$$

where $k_{p,i}$ is the intra-particle diffusion rate constant (mg g$^{-1}$ min$^{1/2}$), and C stand for intercept related to the boundary layer effect (mg g$^{-1}$). The gradient and intercept of the linear plot of $q_t$ versus $t^{1/2}$ (min$^{1/2}$) can be used to compute the $k_p$ and C values.

de Luna et al. (2013) reported that a complex mixture of chemisorption and intra-particle transport could be the rate-limiting step. However, the velocity may be limited by surface diffusion and equilibrium adsorption at different phases, resulting in a multi-linearity in the intra-particle diffusion (Qiu et al. 2009). Figure 11 illustrated the intra-particle diffusion plot and the rate constant $k_{p,i}$ (i = 1, 2, 3) are presented in Table 6.

The graph plot was not linear, and it was made up of three stages with varying slopes with a $\Delta q_e$ value of 12.12%. As observed, the constant rate of the intra-particle diffusion model for three distinct stages was in the order of $k_{p,1} > k_{p,2} > k_{p,3}$. Nevertheless, in the first stage, the plot did not cross the origin. It is
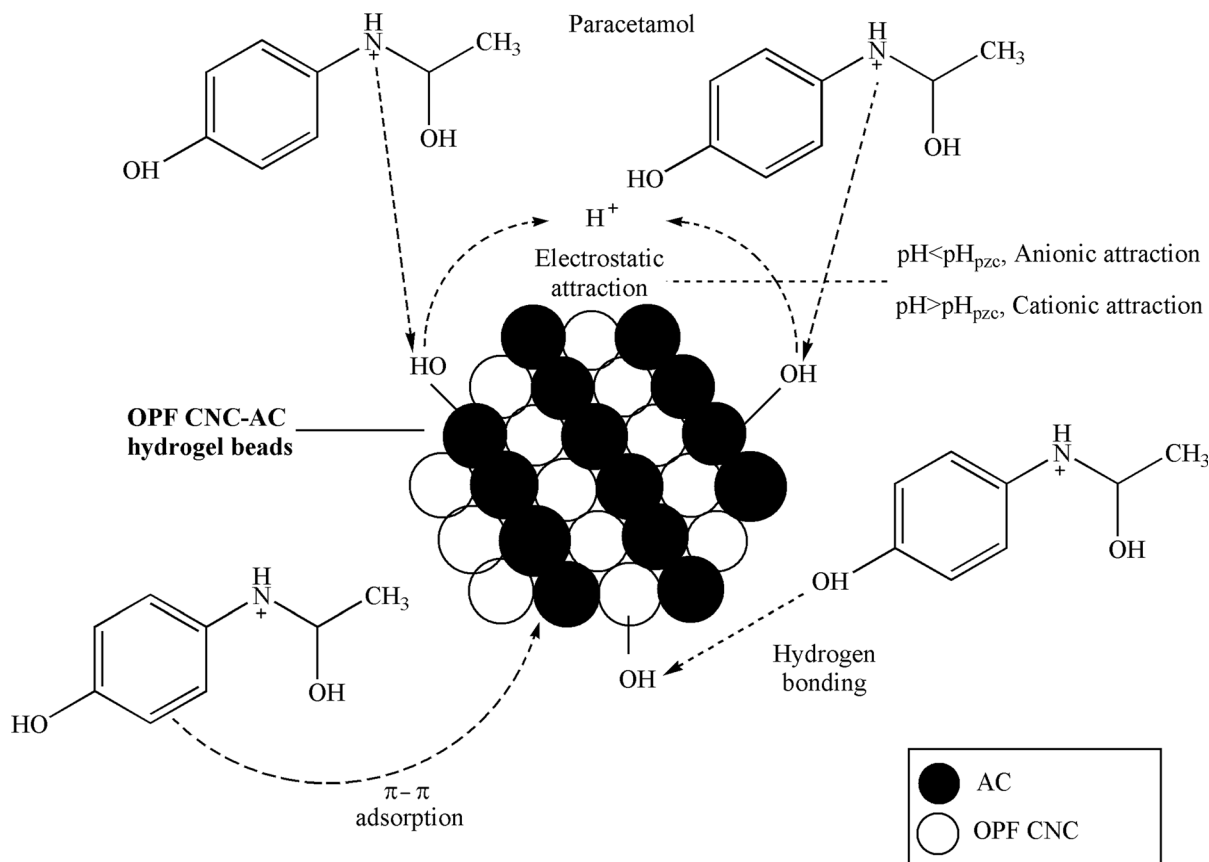
**Fig. 12** Schematic illustration of paracetamol adsorption onto OPF CNC-AC hydrogel beads

claimed that intra-particle diffusion is the only rate-limiting step when the linear plot of $q_t$ versus $t^{1/2}$ ($min^{1/2}$) passes through the origin. However, the current study did not encounter such a phenomenon. In the first stage, the transport of the adsorbate molecules occurs from the bulk phase to the outer surface of the hydrogel beads, which is caused by rapid adsorption, while in the second stage, the adsorbate moves within the adsorbent's pores (Macías-García et al. 2019). In the initial stage, the bead surface was comparatively unoccupied, where the paracetamol molecules that approached the surface of the beads could instantly get adsorbed onto the surface sites. A linear relationship of $q_t$ versus $t^{1/2}$ was observed in the initial adsorption stage, affirming the presence of a diffusion-controlled transport mechanism in paracetamol adsorption onto OPF CNC-AC hydrogel beads. According to the second stage, this period relates to the intra-particle diffusion and the combination of paracetamol molecules with the OPF CNC-AC's

internal adsorption sites. Meanwhile, the third stage depicts the ultimate equilibrium. The distribution tends to reduce due to the reduced adsorbate concentration; adsorption occurs within the adsorbent, and paracetamol molecules have a limited number of adsorption sites to choose from (Macías-García et al. 2019). It was evident that after the initial stage of paracetamol adsorption, the experimental data did not follow the initial trend due to the occupancy of adsorption sites by the already adsorbed paracetamol molecules. Hence, the adsorption rate declined considerably, suggesting the adsorption rate in the latter stage was not diffusion-controlled, rather a binding-controlled process. Similar findings in the adsorption of paracetamol were reported by Wong et al. (2018) and Al-Khateeb et al. (2014).

Therefore, based on the linear regression correlation coefficient ($R^2$) and the normalized standard deviation ($\Delta q_e$) values, the adsorption of paracetamol onto OPF CNC-AC hydrogel beads follows pseudo-
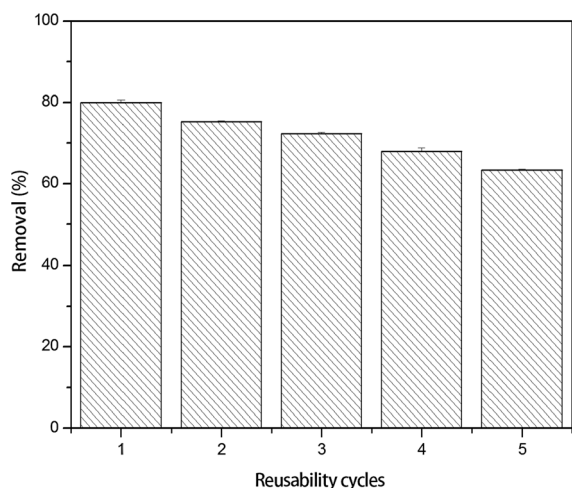
**Fig. 13** Reusability cycles of OPF CNC-AC hydrogel beads

second order and intra-particle diffusion kinetic models since both models contributed the highest $R^2$ and the lowest $\Delta q_e$ values.

### Paracetamol adsorption mechanism by OPF CNC-AC hydrogel beads

Figure 12 illustrates the mechanism of adsorption of paracetamol molecules onto OPF CNC-AC hydrogel beads surface. The adsorption of pharmaceutical substances from an aqueous phase on activated carbon was predominantly due to the interactions between functional groups in the adsorbate structure and groups on the adsorbent surface (Bernal et al. 2017). According to Terzyk (2001), aromatic compounds from aqueous solutions can get adsorbed on activated carbon by three distinct mechanisms: dispersive π electron interactions, formation of hydrogen bonds, and electrostatic interactions. However, π-π interactions appear to be the primary mode of adsorption since the oxygen functional groups can build Lewis acid–base complexes, or hydrogen bonds are lower on activated carbons with changed surface chemistry (Terzyk 2001).

As earlier noted, electrostatic interactions between adsorbent and adsorbate strongly influence the adsorption process of pharmaceutical substances such as paracetamol (Bernal et al. 2017). As a result, changes in the pH of the medium might induce alterations in the adsorbate structure and physicochemical properties of activated carbon. According to Spaltro et al.

(2021), at $pH < pH_{pzc}$, the adsorbent surface is positively charged, favouring anionic species adsorption. In contrast, when the adsorbent is negatively charged, cationic species adsorption is favoured when $pH > pH_{pzc}$.

Paracetamol is a weak electrolyte. It can exist in ionized (a base) and non-ionized (an acid) forms, relying on the solution pH. The OPF CNC-AC hydrogel beads have a positively charged surface at pH 3, whereas paracetamol is neutral (undissociated). At this point, adsorption would be primarily accomplished by π-π interactions between π electrons of the paracetamol molecules' aromatic ring and π electrons of the activated carbon (Spaltro et al. 2021). Apart from that, hydrogen bonding also can occur. The surface of the OPF CNC-AC hydrogel beads is negatively charged at pH 7, and paracetamol is mostly undissociated. Thus, the dominant interactions would be those of π-π interactions between the aromatic rings rather than electrostatic interactions (Spaltro et al. 2021). Meanwhile, at pH 11, the surface of the OPF CNC-AC hydrogel beads also is negatively charged, and paracetamol is mostly ionized (deprotonated). Repulsive electrostatic interactions were involved, resulting in the percentage removal of paracetamol due to the weaker interactions between the surface of the adsorbent and the anionic paracetamol molecules (Mohd et al. 2015). Furthermore, at higher pH, there is competition for adsorption between paracetamol and $OH^-$ onto the adsorbent, contributing to lower adsorption capacity (Dutta et al. 2015).

### Reusability

In determining the efficiency of adsorbents in practical applications, reusability is also an essential factor to be considered. As shown in Fig. 13, the OPF CNC-AC hydrogel beads can be recycled up to five times after the desorption step. Even though the adsorption ability decreased with increasing cycles, the percentage removal of paracetamol was only reduced by 16.57% after five cycles. Fan et al. (2019) stated that some active sites were destroyed during elution or because some adsorption sites remained occupied in the subsequent cycles. The desorption by 5% ethanol also did not complete the recovery of paracetamol ions from the adsorbents, resulting in decreasing percentage removal in second, third, fourth and fifth cycles (Vakili et al. 2019b). Besides, during subsequent

sorption and desorption processes, the adsorbent particles may decompose, thus causing the sorption site to decrease (Daneshvar et al. 2017).

In addition, OPF CNC-AC hydrogel beads showed an excellent result, with 79.98% of paracetamol removal used during the first cycle. However, the percentage removal was reduced to 63.41% during the fifth cycle. Thus, the findings revealed that the OPF CNC-AC hydrogel beads could be reused up to five times, indicating that this adsorbent has strong recyclability, is easily regenerated, and has the potential in wastewater treatment.

## Conclusion

In this study, the hydrogel beads were successfully developed from OPF-CNC and commercial AC to remove paracetamol. The OPF CNC-AC hydrogel beads depended on operational parameters like pH, contact time and the initial paracetamol concentration. The Langmuir, Freundlich, Temkin, and Dubinin-Radushkevich models were used to evaluate the equilibrium adsorption of paracetamol onto OPF CNC-AC hydrogel beads, and the results showed that the Langmuir-1 model suited the experimental data better. The negative value of $\Delta G$ proved that paracetamol molecules were spontaneously adsorbed onto the surface of OPF CNC-AC hydrogel beads, and the physical adsorption dominates the adsorption process as was suggested by the adsorption energy determined by the Dubinin-Radushkevich isotherm model. The pseudo-first order, pseudo-second order, Elovich kinetic, and intra-particle diffusion models were used to analyze the adsorption kinetics. It was revealed that the adsorption of paracetamol onto OPF CNC-AC hydrogel beads follows the pseudo-second order model, with the $R^2$ higher than 0.99. Besides, the hydrogel beads showed good reusability in at least five successive adsorption/desorption cycles. Thus, OPF CNC-AC hydrogel beads may well be used as a promising low-priced, eco-friendly adsorbent to remove paracetamol from wastewater.

## Declarations

## References

Afzal MZ, Sun X-F, Liu J, Song C, Wang S-G, Javed A (2018) Enhancement of ciprofloxacin sorption on chitosan/biochar hydrogel beads. Sci Total Environ 639:560–569. https://doi.org/10.1016/j.scitotenv.2018.05.129

Al-Khateeb LA, Almotiry S, Salam MA (2014) Adsorption of pharmaceutical pollutants onto graphene nanoplatelets. Chem Eng J 248:191–199. https://doi.org/10.1016/j.cej.2014.03.023

Aydin E, Talinli I (2013) Analysis, occurrence and fate of commonly used pharmaceuticals and hormones in the Buyukcekmece Watershed, Turkey. Chemosphere 90:2004–2012. https://doi.org/10.1016/j.chemosphere.2012.10.074

Barthel M et al. (2018) Study on the environmental impact of palm oil consumption and on existing sustainability standards: final report and appendices. Publications Office of the European Union,

Beaumont M, König J, Opietnik M, Potthast A, Rosenau T (2017) Drying of a cellulose II gel: effect of physical modification and redispersibility in water. Cellulose 24:1199–1209. https://doi.org/10.1007/s10570-016-1166-9

Bernal V, Erto A, Giraldo L, Moreno-Piraján JC (2017) Effect of solution pH on the adsorption of paracetamol on chemically modified activated carbons. Molecules 22:1032. https://doi.org/10.3390/molecules22071032

Bhushan B, Apte U (2019) Liver regeneration after acetaminophen hepatotoxicity: mechanisms and therapeutic opportunities. Am J Pathol 189:719–729. https://doi.org/10.1016/j.ajpath.2018.12.006

Binabas MR, Oros DR, Simoneit BRT (2004) Biomass burning as the main source of organic aerosol particulate matter in Malaysia during haze episodes. Chemosphere 55:1089–1095. https://doi.org/10.1016/j.chemosphere.2004.02.002

Blanco A, Monte MC, Campano C, Balea A, Merayo N, Negro C (2018) Nanocellulose for industrial use: cellulose nanofibers (CNF) cellulose nanocrystals (CNC) and bacterial cellulose (BC). In: Handbook of nanomaterials for industrial applications. Elsevier, Berlin, pp 74–126. https://doi.org/10.1016/B978-0-12-813351-4.00005-5

Chen Y, Yu G, Cao Q, Zhang H, Lin Q, Hong Y (2013) Occurrence and environmental implications of

pharmaceuticals in Chinese municipal sewage sludge. Chemosphere 93:1765–1772. https://doi.org/10.1016/j.chemosphere.2013.06.007

Chien SH, Clayton WR (1980) Application of Elovich equation to the kinetics of phosphate release and sorption in soils. Soil Sci Soc Am J 44:265–268. https://doi.org/10.2136/sssaj1980.03615995004400020013x

Chuein L et al (2021) Kinetics and equilibrium studies of methylene blue dye adsorption on oil palm frond adsorbent. Desalin Water Treat 216:358–371. https://doi.org/10.5004/dwt.2021.26795

Coimbra RN, Escapa C, Otero M (2018) Adsorption separation of analgesic pharmaceuticals from ultrapure and waste water: batch studies using a polymeric resin and an activated carbon. Polymers 10:958. https://doi.org/10.3390/polym10090958

Dada AO, Olalekan AP, Olatunya AM, Dada O (2012) Langmuir, Freundlich, Temkin and Dubinin-Radushkevich isotherms studies of equilibrium sorption of Zn2+ unto phosphoric acid modified rice husk. J Appl Chem 3:38–45

Daneshvar E, Vazirzadeh A, Niazi A, Kousha M, Naushad M, Bhatnagar A (2017) Desorption of methylene blue dye from brown macroalga: effects of operating parameters, isotherm study and kinetic modeling. J Clean Prod 152:443–453. https://doi.org/10.1016/j.jclepro.2017.03.119

Diyanilla R, Hamidon TS, Suryanegara L, Hussin MH (2020) Overview of pretreatment methods employed on oil palm biomass in producing value-added products: a review. BioResources 15:9935. https://doi.org/10.15376/biores.15.4.Diyanilla

Dubinin MM, Zaverina ED, Radushkevich LV (1947) Sorption and structure of active carbons. I. Adsorption of organic vapors. Zh Fiz Khim+ 21:151–162.

Dungani R, Aditiawati P, Aprilia S, Yuniarti K, Karliati T, Suwandhi I, Sumardi I (2018) Biomaterial from oil palm waste: properties, characterization and applications. Palm Oil 31:31–51. https://doi.org/10.5772/intechopen.76412

Dutta M, Das U, Mondal S, Bhattachriya S, Khatun R, Bagal R (2015) Adsorption of acetaminophen by using tea waste derived activated carbon. Int J Environ Sci 6:270–281. https://doi.org/10.6088/ijes.6031

Everett DH (1972) Manual of symbols and terminology for physicochemical quantities and units, appendix II: definitions, terminology and symbols in colloid and surface chemistry. Pure Appl Chem 31:577–638. https://doi.org/10.1351/pac197231040577

Fan L, Lu Y, Yang L-Y, Huang F, Ouyang X-k (2019) Fabrication of polyethylenimine-functionalized sodium alginate/cellulose nanocrystal/polyvinyl alcohol core–shell microspheres ((PVA/SA/CNC)@ PEI) for diclofenac sodium adsorption. J Colloid Interface Sci 554:48–58. https://doi.org/10.1016/j.jcis.2019.06.099

Ferchichi M, Dhaouadi H (2016) Sorption of paracetamol onto biomaterials. Water Sci Technol 74:287–294. https://doi.org/10.2166/wst.2016.218

Ferreira RC et al (2015) Adsorption of paracetamol using activated carbon of dende and babassu coconut mesocarp. Int J Biol, Biomole, Agri, Food Biotechnol Eng 9:674–679. https://doi.org/10.5281/zenodo.1106943

Freundlich H (1906) Freundlich's Adsorption Isotherm. J Phys Chem-US 57:384

Fu C, Zhang H, Xia M, Lei W, Wang F (2020) The single/co-adsorption characteristics and microscopic adsorption mechanism of biochar-montmorillonite composite adsorbent for pharmaceutical emerging organic contaminant atenolol and lead ions. Ecotox Environ Safe 187:109763. https://doi.org/10.1016/j.ecoenv.2019.109763

Goel NK, Kumar V, Misra N, Varshney L (2015) Cellulose based cationic adsorbent fabricated via radiation grafting process for treatment of dyes waste water. Carbohydr Polym 132:444–451. https://doi.org/10.1016/j.carbpol.2015.06.054

Gracia-Lor E, Sancho JV, Serrano R, Hernández F (2012) Occurrence and removal of pharmaceuticals in wastewater treatment plants at the Spanish Mediterranean area of Valencia. Chemosphere 87(453):462. https://doi.org/10.1016/j.chemosphere.2011.12.025

Haafiz MKM, Eichhorn SJ, Hassan A, Jawaid M (2013) Isolation and characterization of microcrystalline cellulose from oil palm biomass residue. Carbohydr Polym 93:628–634. https://doi.org/10.1016/j.carbpol.2013.01.035

Habibi Y (2014) Key advances in the chemical modification of nanocelluloses. Chem Soc Rev 43:1519–1542. https://doi.org/10.1039/C3CS60204D

Haitham K, Razak S, Nawi MA (2019) Kinetics and isotherm studies of methyl orange adsorption by a highly recyclable immobilized polyaniline on a glass plate. Arab J Chem 12:1595–1606. https://doi.org/10.1016/j.arabjc.2014.10.010

Hamad BK, Noor AM, Afida AR, Asri MNM (2010) High removal of 4-chloroguaiacol by high surface area of oil palm shell-activated carbon activated with NaOH from aqueous solution. Desalination 257:1–7. https://doi.org/10.1016/j.desal.2010.02.007

Hassan AF, Abdel-Mohsen AM, Fouda MMG (2014) Comparative study of calcium alginate, activated carbon, and their composite beads on methylene blue adsorption. Carbohydr Polym 102:192–198. https://doi.org/10.1016/j.carbpol.2013.10.104

Ho Y-S (2006) Review of second-order models for adsorption systems. J Hazard Mater 136:681–689. https://doi.org/10.1016/j.jhazmat.2005.12.043

Ho YS, McKay G (1998) The kinetics of sorption of basic dyes from aqueous solution by sphagnum moss peat. Can J Chem Eng 76:822–827. https://doi.org/10.1002/cjce.5450760419

Hu D, Jiang R, Wang N, Xu H, Wang Y-G, Ouyang X-k (2019) Adsorption of diclofenac sodium on bilayer amino-functionalized cellulose nanocrystals/chitosan composite. J Hazard Mater 369:483–493. https://doi.org/10.1016/j.jhazmat.2019.02.057

Hu Z-H, Omer AM, Ouyang Xk YuD (2018) Fabrication of carboxylated cellulose nanocrystal/sodium alginate hydrogel beads for adsorption of Pb (II) from aqueous solution. Int J Biol Macromol 108:149–157. https://doi.org/10.1016/j.ijbiomac.2017.11.171

Husein DZ, Hassanien R, Al-Hakkani MF (2019) Green-synthesized copper nano-adsorbent for the removal of pharmaceutical pollutants from real wastewater samples.

Heliyon 5:e02339. https://doi.org/10.1016/j.heliyon.2019.e02339

Hussin MH et al (2016) Physicochemical of microcrystalline cellulose from oil palm fronds as potential methylene blue adsorbents. Int J Biol Macromol 92:11–19. https://doi.org/10.1016/j.ijbiomac.2016.06.094

Javadian H, Ghorbani F, Tayebi H-a, Asl SH (2015) Study of the adsorption of Cd (II) from aqueous solution using zeolite-based geopolymer, synthesized from coal fly ash; kinetic, isotherm and thermodynamic studies. Arab J Chem 8:837–849. https://doi.org/10.1016/j.arabjc.2013.02.018

Jendrzejewska I, Goryczka T, Pietrasik E, Klimontko J, Jampilek J (2020) X-ray and thermal analysis of selected drugs containing acetaminophen. Molecules 25:5909. https://doi.org/10.3390/molecules25245909

Joshi S, Pokharel BP (2013) Preparation and characterization of activated carbon from lapsi (Choerospondias axillaris) seed stone by chemical activation with potassium hydroxide. J I Eng 9:79–88. https://doi.org/10.3126/jie.v9i1.10673

Khader EH, Mohammed TJ, Mirghaffari N, Salman AD, Juzsakova T, Abdullah TA (2021) Removal of organic pollutants from produced water by batch adsorption treatment. Clean Techn Environ Policy. https://doi.org/10.1007/s10098-021-02159-z

Kumar A et al (2017) Effect of crosslinking functionality on microstructure, mechanical properties, and in vitro cytocompatibility of cellulose nanocrystals reinforced poly (vinyl alcohol)/sodium alginate hybrid scaffolds. Int J Biol Macromol 95:962–973. https://doi.org/10.1016/j.ijbiomac.2016.10.085

Lagergren SK (1898) About the theory of so-called adsorption of soluble substances. K Sven Vetenskapsakad Handl 24:1–39

Langmuir I (1918) The adsorption of gases on plane surfaces of glass, mica and platinum. J Am Chem Soc 40:1361–1403. https://doi.org/10.1021/ja02242a004

De Laurentiis E et al (2014) Assessing the photochemical transformation pathways of acetaminophen relevant to surface waters: transformation kinetics, intermediates, and modelling. Water Res 53:235–248. https://doi.org/10.1016/j.watres.2014.01.016

Lei M, Zhang L, Lei J, Zong L, Li J, Wu Z, Wang Z (2015) Overview of emerging contaminants and associated human health effects. BioMed Res Int 2015:404796. https://doi.org/10.1155/2015/404796

Liyanage AS, Canaday S, Pittman CU Jr, Mlsna T (2020) Rapid remediation of pharmaceuticals from wastewater using magnetic Fe3O4/Douglas fir biochar adsorbents. Chemosphere 258:127336. https://doi.org/10.1016/j.chemosphere.2020.127336

de Luna MDG, Briones RM, Su C-C, Lu M-C (2013) Kinetics of acetaminophen degradation by Fenton oxidation in a fluidized-bed reactor. Chemosphere 90:1444–1448. https://doi.org/10.1016/j.chemosphere.2012.09.003

Luo X, Lei X, Cai N, Xie X, Xue Y, Yu F (2016) Removal of heavy metal ions from water by magnetic cellulose-based beads with embedded chemically modified magnetite nanoparticles and activated carbon. Sustain Chem Eng 4:3960–3969. https://doi.org/10.1021/acssuschemeng.6b00790

Macías-García A, García-Sanz-Calcedo J, Carrasco-Amador JP, Segura-Cruz R (2019) Adsorption of paracetamol in hospital wastewater through activated carbon filters. Sustainability 11:2672. https://doi.org/10.3390/su11092672

Martins AC et al (2015) Removal of tetracycline by NaOH-activated carbon produced from macadamia nut shells: kinetic and equilibrium studies. Chem Eng J 260:291–299. https://doi.org/10.1016/j.cej.2014.09.017

Mashayekh-Salehi A, Moussavi G (2016) Removal of acetaminophen from the contaminated water using adsorption onto carbon activated with NH4Cl. Desalin Water Treat 57:12861–12873. https://doi.org/10.1080/19443994.2015.1051588

Maya E, Abdul H, Keong L (2016) Optimization of bioethanol production process using oil palm frond juice as substrate. Malays J Microbiol 12:308–314. https://doi.org/10.21161/mjm.84016

Mohammed N, Grishkewich N, Berry RM, Tam KC (2015) Cellulose nanocrystal–alginate hydrogel beads as novel adsorbents for organic dyes in aqueous solutions. Cellulose 22:3725–3738. https://doi.org/10.1007/s10570-015-0747-3

Mohd N, Sudirman M, Draman SFS (2015) Isotherm and thermodynamic study of paracetamol removal in aqueous solution by activated carbon. J Eng Appl Sci 10:9516–9520

Mompelat S, Le Bot B, Thomas O (2009) Occurrence and fate of pharmaceutical products and by-products, from resource to drinking water. Environ Int 35:803–814. https://doi.org/10.1016/j.envint.2008.10.008

Mouni L et al (2018) Removal of Methylene Blue from aqueous solutions by adsorption on Kaolin: kinetic and equilibrium studies. Appl Clay Sci 153:38–45. https://doi.org/10.1016/j.clay.2017.11.034

Mukoko T (2016) Preparation of rice hull activated carbon for the removal of selected pharmaceutical waste compounds in hospital effluent. J Environ Anal Toxicol. https://doi.org/10.4172/2161-0525.S7-008

Nasrullah A, Bhat AH, Naeem A, Isa MH, Danish M (2018) High surface area mesoporous activated carbon-alginate beads for efficient removal of methylene blue. Int J Biol Macromol 107:1792–1799. https://doi.org/10.1016/j.ijbiomac.2017.10.045

Nche N-AG, Bopda A, Tchuifon DRT, Ngakou CS, Kuete I-HT, Gabche AS (2017) Removal of paracetamol from aqueous solution by adsorption onto activated carbon prepared from rice husk. J Chem Pharm Res 9:56–68

Nguyen DT et al (2020) Adsorption process and mechanism of acetaminophen onto commercial activated carbon. J Environ Chem Eng 8:104408. https://doi.org/10.1016/j.jece.2020.104408

Oladipo AA, Gazi M, Saber-Samandari S (2014) Adsorption of anthraquinone dye onto eco-friendly semi-IPN biocomposite hydrogel: equilibrium isotherms, kinetic studies and optimization. J Taiwan Inst Chem Eng 45:653–664. https://doi.org/10.1016/j.jtice.2013.07.013

Olgun A, Atar N (2009) Equilibrium and kinetic adsorption study of Basic Yellow 28 and Basic Red 46 by a boron industry waste. J Hazard Mater 161:148–156. https://doi.org/10.1016/j.jhazmat.2008.03.064

Patel M, Kumar R, Kishor K, Mlsna T, Pittman CU Jr, Mohan D (2019) Pharmaceuticals of emerging concern in aquatic

systems: chemistry, occurrence, effects, and removal methods. Chem Rev 119:3510–3673. https://doi.org/10.1021/acs.chemrev.8b00299

Phanthong P, Reubroycharoen P, Hao X, Xu G, Abudula A, Guan G (2018) Nanocellulose: extraction and application. Carbon Resour Convers 1:32–43. https://doi.org/10.1016/j.crcon.2018.05.004

Qiu H, Lv L, Pan B-c, Zhang Q-j, Zhang W-m, Zhang Q-x (2009) Critical review in adsorption kinetic models. J Zhejiang Univ Sci A 10:716–724. https://doi.org/10.1631/jzus.A0820524

Raghav S, Kumar D (2018) Adsorption equilibrium, kinetics, and thermodynamic studies of fluoride adsorbed by tetrametallic oxide adsorbent. J Chem Eng Data 63:1682–1697. https://doi.org/10.1021/acs.jced.8b00024

Rieman W, Walton HF (2013) Ion exchange in analytical chemistry: international series of monographs in analytical chemistry. Elsevier

Rivera-Utrilla J, Sánchez-Polo M, Ferro-García MÁ, Prados-Joya G, Ocampo-Pérez R (2013) Pharmaceuticals as emerging contaminants and their removal from water. A Rev Chemo 93:1268–1287. https://doi.org/10.1016/j.chemosphere.2013.07.059

Rogowska J, Zimmermann A, Muszyńska A, Ratajczyk W, Wolska L (2019) Pharmaceutical household waste practices: preliminary findings from a case study in Poland. Environ Manage 64:97–106. https://doi.org/10.1007/s00267-019-01174-7

Setiabudi HD, Jusoh R, Suhaimi S, Masrur SF (2016) Adsorption of methylene blue onto oil palm (Elaeis guineensis) leaves: process optimization, isotherm, kinetics and thermodynamic studies. J Taiwan Inst Chem Eng 63:363–370. https://doi.org/10.1016/j.jtice.2016.03.035

Sikarwar S, Jain R (2014) Kinetics and thermodynamic study of balsalazide adsorption by unsaturated polyester resin (UPR): a non-carbon adsorbent. Water Air Soil Pollut 225:1–10. https://doi.org/10.1007/s11270-013-1842-4

Sim W-J, Lee J-W, Oh J-E (2010) Occurrence and fate of pharmaceuticals in wastewater treatment plants and rivers in Korea. Environ Pollut 158:1938–1947. https://doi.org/10.1016/j.envpol.2009.10.036

Snelgrove LJ (2017) A study on the removal of common analgesics from waste water, using zeolites Clinoptilolite and Beta

Soto ML, Moure A, Domínguez H, Parajó JC (2011) Recovery, concentration and purification of phenolic compounds by adsorption: a review. J Food Eng 105:1–27. https://doi.org/10.1016/j.jfoodeng.2011.02.010

Spaltro A, Pila MN, Colasurdo DD, Grau EN, Román G, Simonetti S, Ruiz DL (2021) Removal of paracetamol from aqueous solution by activated carbon and silica Experimental and computational study. J Contam Hydrol 236:103739. https://doi.org/10.1016/j.jconhyd.2020.103739

Spessato L et al (2019) KOH-super activated carbon from biomass waste: insights into the paracetamol adsorption mechanism and thermal regeneration cycles. J Hazard Mater 371:499–505. https://doi.org/10.1016/j.jhazmat.2019.02.102

Supramaniam J, Adnan R, Kaus NHM, Bushra R (2018) Magnetic nanocellulose alginate hydrogel beads as potential drug delivery system. Int J Biol Macromol 118:640–648. https://doi.org/10.1016/j.ijbiomac.2018.06.043

Tan CHC, Sabar S, Hussin MH (2018) Development of immobilized microcrystalline cellulose as an effective adsorbent for methylene blue dye removal. S Afr J Chem Eng 26:11–24. https://doi.org/10.1016/j.sajce.2018.08.001

Terzyk AP (2001) The influence of activated carbon surface chemical composition on the adsorption of acetaminophen (paracetamol) in vitro: Part II. TG, FTIR, and XPS analysis of carbons and the temperature dependence of adsorption kinetics at the neutral pH. Colloids Surf A Physicochem Eng Asp 177:23–45. https://doi.org/10.1016/S0927-7757(00)00594-X

Trache D, Hussin MH, Haafiz MKM, Thakur VK (2017) Recent progress in cellulose nanocrystals: sources and production. Nanoscale 9:1763–1786. https://doi.org/10.1039/C6NR09494E

Trache D, Tarchoun AF, Derradji M, Hamidon TS, Masruchin N, Brosse N, Hussin MH (2020) Nanocellulose: from fundamentals to advanced applications. Front Chem 8:392. https://doi.org/10.3389/fchem.2020.00392

Trivedi MK, Patil S, Shettigar H, Bairwa K, Jana S (2015) Effect of biofield treatment on spectral properties of paracetamol and piroxicam. Chem Sci J. https://doi.org/10.4172/2150-3494.100098

Tsai W-T, Hsien K-J, Hsu H-C (2009) Adsorption of organic compounds from aqueous solution onto the synthesized zeolite. J Hazard Mater 166:635–641. https://doi.org/10.1016/j.jhazmat.2008.11.071

Vakili M et al (2019a) Ultrasound-assisted preparation of chitosan/nano-activated carbon composite beads aminated with (3-aminopropyl) triethoxysilane for adsorption of acetaminophen from aqueous solutions. Polymers 11:1701. https://doi.org/10.3390/polym11101701

Vakili M, Deng S, Shen L, Shan D, Liu D, Yu G (2019b) Regeneration of chitosan-based adsorbents for eliminating dyes from aqueous solutions. Sep Purif Rev 48:1–13. https://doi.org/10.1080/15422119.2017.1406860

Wadhah Hassan AE (2017) Occurrence of paracetamol in aquatic environments and transformation by microorganisms: a review. Chron Pharm Sci 1:341–355

Weber WJ Jr, Morris JC (1963) Kinetics of adsorption on carbon from solution. J Sanit Eng Div 89:31–59. https://doi.org/10.1061/JSEDAI.0000430

Wong S et al (2018) Removal of acetaminophen by activated carbon synthesized from spent tea leaves: equilibrium, kinetics and thermodynamics studies. Powder Technol 338:878–886. https://doi.org/10.1016/j.powtec.2018.07.075

World Health O (2012) Pharmaceuticals in drinking-water

Yadav S et al (2020) Cationic dye removal using novel magnetic/activated charcoal/β-cyclodextrin/alginate polymer nanocomposite. Nanomaterials 10:170. https://doi.org/10.3390/nano10010170

Yamuna RT, Namasivayam C (1993) Color removal from aqueous solution by biogas residual slurry. Toxicol Environ Chem 38:131–143. https://doi.org/10.1080/02772249309357884

Yan Q et al (2014) Occurrence and fate of pharmaceutically active compounds in the largest municipal wastewater treatment plant in Southwest China: mass balance analysis

and consumption back-calculated model. Chemosphere 99:160–170. https://doi.org/10.1016/j.chemosphere.2013.10.062

Yu Z, Peldszus S, Huck PM (2008) Adsorption characteristics of selected pharmaceuticals and an endocrine disrupting compound—Naproxen, carbamazepine and nonylphenol-on activated carbon. Water Res 42:2873–2882. https://doi.org/10.1016/j.watres.2008.02.020

Çeçen F (2014) Activated carbon. In Kirk-Othmer Encyclopedia of Chemical Technology:1–34. doi:https://doi.org/10.1002/0471238961.0103200902011105.a01.pub3